

VecComp: Vector Computing via MIMO Digital Over-the-Air Computation

Saeed Razavikia, *Member, IEEE*, José Mairton Barros Da Silva Junior, *Member, IEEE*, Carlo Fischione, *Fellow, IEEE*

Abstract—Recently, the ChannelComp framework has proposed digital over-the-air computation by designing digital modulations that enable the computation of arbitrary functions. Unlike traditional analog over-the-air computation, which is restricted to nomographic functions, ChannelComp enables a broader range of computational tasks while maintaining compatibility with digital communication systems. This framework is intended for applications that favor local information processing over the mere acquisition of data. However, ChannelComp is currently designed for scalar function computation, while numerous data-centric applications necessitate vector-based computations, and it is susceptible to channel fading. In this work, we introduce a generalization of the ChannelComp framework, called VecComp, by integrating ChannelComp with multiple-antenna technology. This generalization not only enables vector function computation but also ensures scalability in the computational complexity, which increases only linearly with the vector dimension. As such, VecComp remains computationally efficient and robust against channel impairments, making it suitable for high-dimensional, data-centric applications. We establish a non-asymptotic upper bound on the mean squared error of VecComp, affirming its computation efficiency under fading channel conditions. Numerical experiments show the effectiveness of VecComp in improving the computation of vector functions and fading compensation over noisy and fading multiple-access channels.

Index Terms—Digital modulation, over-the-air computation, MIMO systems, massive MIMO, and vector computation.

I. INTRODUCTION

Over-the-air computation (OAC) emerges at the confluence of computation and communication domains. OAC facilitates the computation of mathematical functions by leveraging the superposition characteristic of wireless multiple access channel (MAC) [1]. This leads to a high-rate data aggregation protocol that can potentially be essential for the next generation of communication networks, catering to applications such as the Internet of Things (IoT) and edge machine learning [2].

OAC, initially focused on analog modulation [3], [4], faces challenges with digital modulation due to nonlinearity and lack of digital coding, impacting reliability and compatibility with digital systems. Recent research addresses these issues by developing basic digital OAC design for a specific function [5].

S. Razavikia and C. Fischione are with the School of Electrical Engineering and Computer Science KTH Royal Institute of Technology, Stockholm, Sweden (e-mail: sraz@kth.se, carlofi@kth.se). C. Fischione is also with Digital Futures of KTH.

José Mairton B. da Silva Jr. is with the Department of Information Technology, Uppsala University, Sweden (email: mairton.barros@it.uu.se).

S. Razavikia was supported by the Wallenberg AI, Autonomous Systems and Software Program (WASP), and Ericsson Research Foundation.

The SSF SAICOM project and the SweWIN research center partially supported this work

Further advancements that we have conducted have established OAC's compatibility with digital channel coding and generalized digital modulation [6], [7]; our recent results enable reliable computation and aggregation results, enhancing OAC's robustness and efficiency in modern digital communication systems.

In modern wireless networks, multiple-input multiple-output (MIMO) has become the basic technology for improving wireless transceiver performance [8]. Multiple antennas at both the transmitter and receiving sides increase spectral efficiency, expand range, and strengthen link reliability. If a transmitting node only uses a single antenna, in OAC, we can only compute a single function per available communication resources, such as bandwidth or time slots. However, the next generation of wireless networks with MIMO will allow the simultaneous processing of multi-function purposes, such as matrix-based computation. This motivates us to investigate OAC techniques for MIMO systems in MAC. OAC for MIMO can potentially perform multiple calculations simultaneously and reduce errors using spatial diversity. As a result, the time needed for data combination in computation networks can be reduced. This helps meet the low latency requirements of future networks, especially when high mobility is involved. Complex matrix calculations for machine learning and distributed computing could thus be achieved.

A. Literature Review

In the seminal works by [1], [4], the computing principles across MAC have been systematically studied, focusing on the theoretical limits for a predefined many-to-one function. In [3], [9], the authors have established a connection between OAC and nomographic functions and expanded the range of functions that OAC can compute, including a set broader than merely linear functions. This connection has shown that OAC offers a superior computation rate compared to isolated communication and computation processes. Due to these promising theoretical findings, the OAC framework has garnered increased attention. The domain of OAC has been investigated from diverse perspectives, such as information theory [10], signal processing [3], and synchronization challenges [11]–[13]. Notably, the analog method OAC has been recognized for its potential to optimize communication resources, especially in federated edge learning [14].

However, dependency on analog communication makes the reliability of OAC questionable due to the wireless channel distortions and noise [15]. Moreover, its dependence on

analog hardware is limiting, given the few modern devices supporting analog modulations [6], [16]. Towards devising a digital aggregation method, one-bit broadband digital aggregation, using simple binary phase shift keying modulation, has been introduced in [5] with its extension to non-coherent system model studied in [15], [17]. However, the highlighted efforts predominantly focus on particular functions and are confined to specific machine learning training methods, such as signSGD [18]. Towards boosting reliability, the works in [19], [20] introduce zero-forcing beamforming, which mitigates interference in analog OAC systems. In contrast, [21] proposes hybrid beamforming for massive MIMO OAC, leveraging spatial diversity to enhance computational accuracy. A significant advancement is presented in [22], which formulates an optimal transceiver beamforming design for multi-antenna transmitters and receivers. Similarly, [23] studies OAC in cell-free MIMO systems, analyzing the impact of network cooperation on computational accuracy. These studies demonstrate the potential of MIMO to improve OAC performance but remain constrained to analog transmission, which is inherently susceptible to noise accumulation. Furthermore, their beamforming designs presume perfect CSI at both transmitters and receiver ends and impose stringent synchronization requirements.

Most existing OAC frameworks are designed to compute scalar functions, typically nomographic functions that can be expressed as summations of local components. While effective for applications such as federated learning [14] and distributed sensing [20], these methods are not directly applicable to more general vector function computations, such as nonlinear activation functions in neural network architecture.

In recent works [6], [7], [24]–[27], we have presented the ChannelComp framework, a novel communication for computation paradigm. The ChannelComp framework enables the computation of various functions over the MAC utilizing digital modulations. The ChannelComp provides a spectral efficient communication approach via digital modulation for the OAC challenge. Moreover, ChannelComp offers computational advantages over analog OAC techniques and integrates seamlessly with digital communication infrastructures [28]. Building on the ChannelComp concept, recent works [29], [30], have explored channel coding techniques within digital OAC to bolster communication reliability.

While ChannelComp has pioneered a new avenue for performing computations via communication, it assumes networks with single antennas, thus performing scalar output functions. Furthermore, ChannelComp has not factored in fading channels within its computational framework, potentially leading to unreliable communication and subsequent computation inaccuracies during outage instances.

Here, we aim to generalize ChannelComp’s computational capabilities by integrating vector computation by incorporating MIMO design. Including MIMO widens the dimensions of computation in ChannelComp, increases spectral efficiency, and reinforces computation accuracy.

However, generalizing ChannelComp to support vector function computation in digital OAC over MIMO systems introduces several fundamental challenges. We outline the key challenges as follows:

- **Vector computation in multi-antenna systems:** While conventional OAC handles only scalar aggregation, extending it to vector functions requires new designs that guarantee separability across multiple output dimensions.
- **CSI-unaware design:** Many existing digital OAC frameworks rely on full CSI at the transmitters to optimize signal transmission. However, acquiring CSI at distributed nodes introduces significant overhead and delays, making real-time computation challenging.
- **Scalability in high-dimensional computation:** As the number of inputs and nodes grows, ChannelComp constraints can increase exponentially, posing challenges to maintaining computational accuracy.
- **Compensation for correlated channels:** In practical multi-antenna systems, channel coefficients often exhibit spatial correlation, deviating from the idealized independent and identically distributed (i.i.d.) assumption. This correlation affects the superposition property of OAC, making it more difficult to achieve reliable function computation.

The following section presents our contributions, which address these challenges and provide a structured approach to advancing digital over-the-air computation in MIMO systems.

B. Our Contributions

This paper proposes extending the ChannelComp scheme, termed VecComp, enabling computing matrix-based functions over a finite field through fading MACs. Notably, the VecComp uses MIMO to provide reliable communication and spectral efficiency with low latency, resulting in a high rate for both matrix- and vector-based function computation. The VecComp framework notably eliminates the need for network nodes to be aware of the channel state information (CSI). This represents a clear evolution from traditional methods used in OAC via a wireless fading MAC. Typically, each transmitting node adjusts its transmission based on the real-time channel state to ensure consistent power level convergence at the receiver. By incorporating multiple antennas at the receiver, VecComp diminishes the fading effects intrinsic to communication channels, reinforcing its functional capacity. Additionally, we analyze the theoretical effectiveness of the VecComp framework. An in-depth analysis is studied to ascertain the required antennas at the receiver for effectively nullifying the wireless channel’s fading characteristics.

Specifically, our contributions are as follows:

- **MIMO-based digital OAC for vector computation:** We introduce VecComp, which extends scalar OAC to vector functions by decoupling channel compensation from compaction. Its complexity grows only linearly with the number of functions and exploits MIMO to compute multiple outputs simultaneously.
- **CSI-unaware OAC computation:** VecComp uses receiver-side CSI and multi-antenna diversity to counter small scale fading, eliminating the need for transmitter CSI and thus reducing delay and boosting spectral efficiency.

- **Handling correlated fading channels:** We quantify how spatial correlation degrades computation accuracy and show that our beamforming strategy effectively mitigates these effects in realistic fading environments.
- **Theoretical guarantees:** We provide the analysis for the required number of antennas N_r at the receiver to obtain an upper bound for the function's computation error to a certain level ϵ . In particular, we derive a probabilistic lower bound on the required receiver antennas, proving $N_r = \mathcal{O}(1/\epsilon^2)$ to ensure an error tolerance ϵ .
- **Numerical experiments:** We validate the theoretical results and assess the VecComp framework's performance effectiveness via extensive numerical experiments. These experiments provide numerical results regarding the computation performance and the proposed fading compensation. Simulation results confirm the theoretical bounds and show that increasing N_r can cut computation error by up to 75%.

Finally, VecComp is a fully digital OAC framework, meaning that it can be directly integrated into modern wireless systems that support digital modulations (e.g., QAM, PSK). This makes it suitable for deployment in cellular networks, IoT applications, and edge computing.

C. Document Organization

The rest of the paper is organized as follows: in Section II, we explain the system model, including the signal models. Next, we give the problem formulation and the methodology for performing the computation over the MAC in Section III. In Section IV, we introduce the proposed VecComp method for computing multiple functions over the MAC. Then, we evaluate the performance of VecComp in terms of MSE over fading and noisy channels in Section VI. Finally, we conclude the paper in Section VII.

D. Notation

We denote a finite field by \mathbb{F}_Q , where Q denotes the number of elements inside the field. Moreover, we denote by \mathbb{Z} , \mathbb{R} , and \mathbb{C} as the integer, real, and complex number sets, respectively. We use lowercase letters x for scalar and calligraphic notation \mathcal{X} to represent operators. The transpose and Hermitian of a matrix \mathbf{X} are represented by \mathbf{X}^T and \mathbf{X}^H , respectively. For a vector \mathbf{x} , $\|\mathbf{x}\|_1$, $\|\mathbf{x}\|_2$ are defined as the ℓ_1 and ℓ_2 vector norms, respectively. We define $\|\mathbf{X}\|$ and $\|\mathbf{X}\|_F$ as the spectral and Frobenius norms of the matrix \mathbf{X} , respectively. For an integer N , $[N]$ corresponds to the set $\{1, 2, \dots, N\}$. We define \mathcal{W}_f as the range of function f , and its cardinality by $|\mathcal{W}_f|$. We use $\mathbf{X} \geq \mathbf{0}$ to show that \mathbf{X} is a positive semidefinite matrix. Finally, we define the $\text{diag} : \mathbb{C}^N \mapsto \mathbb{C}^{N \times N}$ operator over a vector $\mathbf{x} \in \mathbb{C}^N$ as the mapping to a diagonal matrix whose diagonal elements are the entries of vector \mathbf{x} . The null-space of linear operator \mathcal{X} is denoted by $\mathcal{N}(\mathcal{X})$. We define the linear block diagonal operator \mathcal{T} as the direct sum of operators $\{\mathcal{X}_i\}_{i=1}^L$, denoted by $\mathcal{T} := \bigoplus_{i=1}^L \mathcal{X}_i$, where for a complex vector $d = (d_1, \dots, d_L) \in \mathbb{C}^L$, the operator \mathcal{T} is applied component-wise, yielding the output $\mathcal{T}(d) = [\mathcal{X}_1(d_1), \dots, \mathcal{X}_L(d_L)]$.

II. SYSTEM MODEL AND PROBLEM FORMULATION

A. System Model

We have a communication system involving a computation point (CP) with N_r receiver antennas. Also, there are K nodes with N_t transmitter antennas and a single receiver antenna. The nodes communicate with the CP using a shared communication channel. We consider that node k owns value $s_k \in \mathbb{F}_Q$, where Q denotes the number of elements inside the input domain field \mathbb{F}_Q . The objective of the CP is to compute the desired function $\mathbf{f}(s_1, \dots, s_K) : \mathbb{F}_Q^K \mapsto \mathbb{R}^L$ or, $\mathbf{f}(\mathbf{s})$ in short, with L outputs. Note that L must be lower than the number of receiver and transmitter antennas, i.e., $L \leq \min\{N_r, N_t\}$ ¹. In the notable case of $L = 1$, the computation problem would be reduced to the ChannelComp [6] scalar function problem. Therefore, in this paper, we extend the computation problem to a vector function instead of a scalar function, using beamformers at transmitters and receivers to decrease distortion. As an illustrative example, we present the following affine function \mathbf{f} for the given input vector $\mathbf{s} \in \mathbb{F}_Q^K$,

$$\mathbf{f}(\mathbf{s}) = \mathbf{A}\mathbf{s} + \mathbf{b} \in \mathbb{R}^L, \quad (1)$$

where $\mathbf{A} \in \mathbb{R}^{L \times K}$, $\mathbf{b} \in \mathbb{R}^L$. Here, element k of the input vector, s_k , corresponds to data of node k , for $k \in [K]$; and element ℓ of the output vector, $[\mathbf{f}]_\ell$, corresponds to the data received by antenna ℓ at the receiver, accordingly.

Throughout digital transmission process, the value s_k at node k is mapped to L different digitally modulated signal $x_{k,\ell}$ via the encoder $\mathcal{E}_{k,\ell}(\cdot)$ such that $x_{k,\ell} = \mathcal{E}_{k,\ell}(s_k)$, for $\ell \in [L]$. Let $\mathbf{V}_k \in \mathbb{C}^{N_t \times L}$ be the transmit beamforming matrix at node k and let $\mathbf{U} \in \mathbb{C}^{N_r \times L}$ be the receiver beamforming matrix (see Figure 1). Then, the nodes transmit their respective \mathbf{x}_k values, where $\mathbf{x}_k = [x_{k,1}, \dots, x_{k,L}]^T \in \mathbb{C}^L$, using beamforming matrix \mathbf{V}_k over MAC to compute the function \mathbf{f} at the CP. In particular, assuming symbol-level synchronization, all users transmit their symbol vectors simultaneously using their arrays. Then, the measured signal received by the CP over the MAC is given by

$$\mathbf{y} = \mathbf{U}^H \left(\sum_{k=1}^K \frac{\mathbf{H}_k}{N_t} \mathbf{V}_k \mathbf{x}_k + \mathbf{z} \right), \quad (2)$$

where $\mathbf{z} \in \mathbb{C}^{N_r}$ denotes the AWGN vector with i.i.d. distribution from $\mathcal{CN}(0, \sigma_z^2 \mathbf{I}_{N_r})$, and $\mathbf{H}_k \in \mathbb{C}^{N_r \times N_t}$ denotes the MIMO channel matrix for the link from node k to the CP, whose entries are generated i.i.d from complex Normal distribution, i.e. $\mathbf{H}_k \sim \mathcal{CN}(\mathbf{0}, \sigma_{h,k}^2 \mathbf{I}_{N_r})$. The distortion of the received vector concerning the target function vector due to the MIMO channel and noise is suppressed using transmit and receive beamforming. In other words, joint beam formation attempts to combine K symbol vectors in the CP coherently. To compute the function \mathbf{f} , we use an operator \mathcal{T} to map the resultant constellation diagram of signal \mathbf{y}

¹This condition is unavoidable for perfect recovery of $\sum_k \mathbf{x}_k$ over MAC because it is a fundamental limitation dictated by MIMO linear algebra, regardless of the \mathbf{x}_k values. Nevertheless, by adopting wideband transmission over multiple time slots or frequency bands [30], [31], it is possible to increase the number of computational streams beyond the constraints imposed by the per-device antenna count. When bandwidth is restricted, a wait-and-transmit strategy [32] can be adopted to alleviate this constraint.

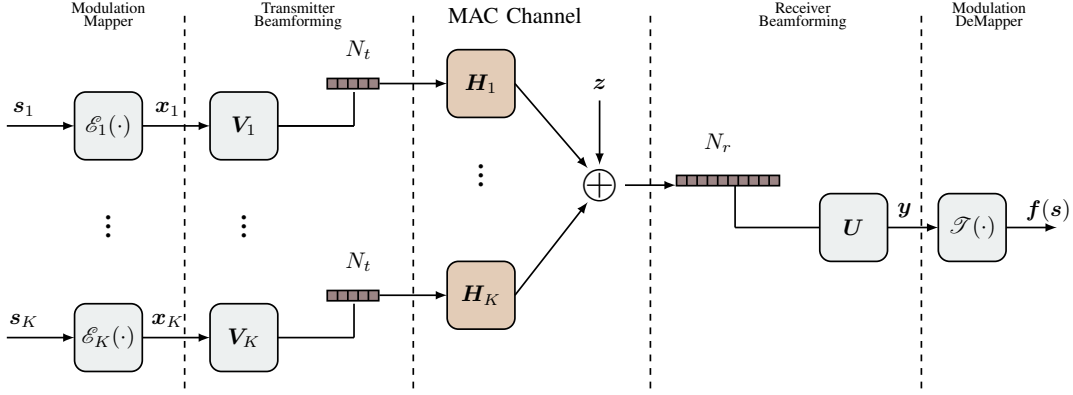


Figure 1. MIMO Setup with k transmitters, where there are N_t transmitter antenna at nodes and N_r receivers antenna at the CP. Node k uses a beamforming matrix $\mathbf{V}_k \in \mathbb{C}^{N_t \times L}$ to transmit the signal \mathbf{x}_k derived from the encoded source signal \mathbf{s}_k via the encoder $\mathcal{E}_k(\cdot)$. The signal passes through the channel matrix \mathbf{H}_k and is combined into the additive noise, z , thus representing the aggregated received signal. The received signal is then processed by the beamforming matrix \mathbf{U} to produce the final output \mathbf{y} .

to the range of the function \mathbf{f} , i.e., $\mathcal{T}(\mathbf{y}) = \mathbf{f}(\mathbf{s})$, where $\mathbf{s} := [s_1, \dots, s_K]^T \in \mathbb{F}_Q^K$.

Note that each component within the \mathbf{y} constellation diagram is influenced by three processes: the summation given in (2), the number of the nodes K , and the selected modulations for each \mathbf{x}_k . Note that other factors impact the constellation diagram of \mathbf{y} , such as the transmitter beamforming \mathbf{V}_k and the receiver beamforming matrix \mathbf{U} . Consequently, the resulting constellation diagram represents a transformation of the transmitting nodes' original constellation diagram, denoted as \mathbf{x}_k , modulated by the receiver beamforming matrix \mathbf{U} operations.

Remark 1. Several non-idealities must be considered in practical implementations of VecComp, including synchronization errors, carrier frequency offset, multipath fading, channel estimation inaccuracies at the CP, and noise distribution [28]. These factors can impact the accuracy of OAC by introducing phase and amplitude misalignments in the aggregated signal. However, various techniques, such as non-coherent aggregation [12], retransmission strategy [31], and bit slicing [29], can mitigate these effects. VecComp exhibits inherent robustness against such errors due to its beamforming-based design and the randomization introduced in the transmission process. The randomized beamforming technique, which will be discussed in Section III-A, ensures that small synchronization mismatches do not destructively affect the computation accuracy, making VecComp a practical and resilient solution for real-world wireless computation systems.

B. Problem Formulation

If we can appropriately choose the modulation vectors $\mathbf{x}_1, \dots, \mathbf{x}_K$, the mapping $\mathcal{T}(\mathbf{y})$ can be determined based on the diagram of the resultant constellation points by $\sum_k \mathbf{x}_k$ such that its output approximates the value of function \mathbf{f} . Hence, to obtain the sought modulation vectors $\mathbf{x}_1, \dots, \mathbf{x}_K$, we propose

the following optimization problem.

$$\mathcal{P}_0 := \min_{\substack{\mathbf{U}, \mathbf{V}_1, \dots, \mathbf{V}_K \\ \mathbf{x}_1, \dots, \mathbf{x}_K}} \sum_{\mathbf{s} \in \mathcal{D}_f} \|\mathbf{f}(\mathbf{s}) - \mathcal{T}(\mathbf{y})\|_2^2, \\ \text{s.t. } \frac{\|\mathbf{V}_k \mathbf{x}_k\|_2}{N_t} \leq P_{\max}, \quad k \in [K], \quad (3)$$

where P_{\max} is the available power budget at the nodes, and \mathcal{D}_f is the domain of function \mathbf{f} . The bilinear product $\mathbf{V}_k \mathbf{x}_k$ and nonlinear operators \mathcal{E}_k make Problem \mathcal{P}_0 non-convex and highly challenging. To solve this problem, we use a *separation scheme* to design beamforming matrices at the transmitter and receiver, thus helping to compensate for the communication channel's fading and noise effects. Subsequently, we propose the encoders \mathcal{E}_k accordingly to the decoder \mathcal{T} to perform the vector computation through over-the-air computation (OAC) in digital MIMO communications. In the next section, we proceed with the methodology for the fading channel compensation.

III. STATISTICAL CHANNEL COMPENSATION

In this section, we design the beamforming matrices for a scenario where the transmitter nodes are unaware of CSI. Consequently, we use the zero-forcing technique at the CP and consider the asymptotic massive MIMO phenomena for compensating the channel effects. Then, we analyze the efficiency of such a fading channel compensation in terms of the mean square of the computation error.

A. CSI-Unaware Fading Compensation via Beamforming

Without loss of generality, we assume the modulated signals are normalized, i.e., $\|\mathbf{x}_k\|_2^2 = 1$, for $k \in [K]$. Consequently, from the power constraints in (3), the norm of the beamforming matrix \mathbf{V}_k is constrained by the power budget P_{\max} , such that $\|\mathbf{V}_k\| \leq P_{\max} N_t$ for all $k \in [K]$. To compensate for the fading effect, all the nodes generate the beamforming matrices \mathbf{V}_k 's according to a given distribution \mathcal{F}_k obeying the isotropy and incoherence properties discussed shortly. Assume that the CP has access to the perfect CSI and the beamforming matrices

for all the K nodes, i.e., \mathbf{H}_k and \mathbf{V}_k for $k \in [K]$. Regardless of distributions \mathcal{F}_k s, the CP can set $\mathbf{U} = \sum_{k=1}^K \mathbf{V}_k^H \mathbf{H}_k^H / N_r$, which yields the following equation:

$$\mathbf{y} = \frac{1}{\beta} \sum_{k=1}^K \mathbf{V}_k^H \mathbf{H}_k^H \mathbf{H}_k \mathbf{V}_k \mathbf{x}_k + \frac{1}{\beta} \sum_{k,k',k \neq k'}^K \mathbf{V}_{k'}^H \mathbf{H}_{k'}^H \mathbf{H}_k \mathbf{V}_k \mathbf{x}_k + \frac{1}{\beta} \sum_{k=1}^K \mathbf{V}_k^H \mathbf{H}_k^H \mathbf{z}, \quad (4)$$

where we define $\beta = N_r N_t$ as the normalizing factor. Then, we can rewrite (4) as follows: $\mathbf{y} = \mathbf{y}_{\text{sig}} + \mathbf{y}_{\text{inter}} + \mathbf{y}_{\text{noise}}$, where the signal terms belong to \mathbb{C}^L and are given by

$$\mathbf{y}_{\text{sig}} := \frac{1}{\beta} \sum_{k=1}^K \mathbf{V}_k^H \mathbf{H}_k^H \mathbf{H}_k \mathbf{V}_k \mathbf{x}_k, \quad (5a)$$

$$\mathbf{y}_{\text{inter}} := \frac{1}{\beta} \sum_{k,k',k \neq k'}^K \mathbf{V}_{k'}^H \mathbf{H}_{k'}^H \mathbf{H}_k \mathbf{V}_k \mathbf{x}_k, \quad (5b)$$

$$\mathbf{y}_{\text{noise}} := \frac{1}{\beta} \sum_{k=1}^K \mathbf{V}_k^H \mathbf{H}_k^H \mathbf{z}. \quad (5c)$$

Here, \mathbf{V}_k is generated according to some distribution \mathcal{F}_k for $k \in [K]$. To reduce the variance of the interference term $\mathbf{y}_{\text{inter}}$ and increase the power of signal term \mathbf{y}_{sig} , we consider the distribution \mathcal{F}_k to obey the *isotropy* and *independency* properties [33], [34]. Specifically, we assume that the distribution of \mathbf{V}_k s generated from \mathcal{F}_k satisfy the following properties:

$$\textit{Isotropy property: } \mathbb{E}[\mathbf{V}_k^H \mathbf{V}_k] = \sigma_{v,k}^2 N_t \mathbf{I}_L, \quad \mathbf{V}_k \sim \mathcal{F}_k, \quad (6)$$

$$\textit{Independency property: } \mathbb{E}[\mathbf{V}_k^H \mathbf{V}_{k'}] = \mathbf{0}_L, \quad \mathbf{V}_{k'} \sim \mathcal{F}_{k'}, \quad (7)$$

for $k, k' \in [K]$, $k \neq k'$. Therefore, \mathbf{V}_k 's are independent and isotropic random matrices. Note that the power constraints in (3) give a lower bound on the power budget, i.e., $P_{\text{max}} \geq \max_k \sigma_{v,k} / N_t$.

1) *Uncorrelated Fading Channels*: For massive MIMO systems, i.e., $N_r, N_t \rightarrow \infty$, the high-dimensional distributions of matrices $\mathbf{H}_k^H \mathbf{H}_k$ asymptotically follow the Marchenko-Pastur law distribution [35], thus leading to Bai-Yin laws [36], [37] for the extreme eigenvalue of the matrix $\mathbf{H}_k^H \mathbf{H}_k$ with Wishart distribution. Specifically, as the dimensions N_r, N_t increase to infinity while the aspect ratio N_t/N_r is kept fixed, the following relations between the maximum and minimum eigenvalues of the matrix $\mathbf{H}_k^H \mathbf{H}_k$ hold [36], [37]:

$$\lambda_{\min}(\mathbf{H}_k^H \mathbf{H}_k) \approx (N_r - \sqrt{N_t}) \sigma_{h,k}^2, \quad (8a)$$

$$\lambda_{\max}(\mathbf{H}_k^H \mathbf{H}_k) \approx (N_r + \sqrt{N_t}) \sigma_{h,k}^2, \quad (8b)$$

for $k \in [K]$. Moreover, the eigenvalues of Gaussian matrices \mathbf{H}_k based on Wigner's semicircle law yield the following results on the largest eigenvalues, also known as Tracy-Widom law [38]:

$$\lambda_{\max}(\mathbf{H}_k) \rightarrow (\sqrt{N_r} + \sqrt{N_t}) \sigma_{h,k}, \quad k \in [K]. \quad (9)$$

Note that when $N_t/N_r \rightarrow 0$ for a relatively large number of antennas at the CP, i.e., $N_r \gg 1$, we obtain the following

properties [39]:

$$\frac{\mathbf{H}_{k'}^H \mathbf{H}_k}{N_r} \approx \mathbf{0}, \quad \forall k, k' \in [K], \quad k \neq k', \quad (10a)$$

$$\frac{\mathbf{H}_k^H \mathbf{H}_k}{N_r} \approx \sigma_{h,k}^2 \mathbf{I}_{N_t}, \quad \forall k \in [K], \quad (10b)$$

$$\frac{\mathbf{H}_k^H \mathbf{z}}{N_r} \approx \mathbf{0}, \quad \forall k \in [K], \quad (10c)$$

where $\sigma_{h,k}^2$ denotes the path loss from node k to the CP. Note that the large-scale fading coefficients are assumed to be the same for different antennas at the same node but are node-dependent [40]. Therefore, we have the following remark.

Remark 2. *In a high dimensional regime where transmitters and the receiver possess a large number of antennas, i.e., $N_r, N_t \gg 1$, (8b) and (9) state that the eigenvalues of matrices $\mathbf{H}_k^H \mathbf{H}_k / N_r$ and $\mathbf{H}_{k'}^H \mathbf{H}_k$ concentrate around $(1 - \sqrt{N_t}/N_r) \sigma_{h,k}$ and zero, respectively for $k = k'$ and $k \neq k', k, k' \in [K]$. Therefore, by setting $\sqrt{N_t}/N_r \approx 0$, we can asymptotically reduce the fluctuations around the expected values $(1 - \sqrt{N_t}/N_r) \sigma_{h,k}$, which removes the effects of small scale fading from the wireless channels.*

By substituting (10) into (4), the term $\mathbf{y}_{\text{inter}}$ asymptotically goes to zero and we obtain

$$\mathbf{y} \approx \frac{N_r}{\beta} \sum_{k=1}^K \sigma_{h,k}^2 \mathbf{V}_k^H \mathbf{V}_k \mathbf{x}_k. \quad (11)$$

Using the isotropy property of beamforming matrices, then $\mathbf{V}_k^H \mathbf{V}_k \approx \sigma_{v,k}^2 N_t \mathbf{I}_L$. Also, to compensate for the large-scale fading, we set $\sigma_{v,k}^2 = 1/\sigma_{h,k}^2$ for all $k \in [K]$. Hence, we denote the approximate received symbols as

$$\hat{\mathbf{r}} \approx \sum_{k=1}^K \mathbf{x}_k. \quad (12)$$

Hence, we can recover the sum signal $\sum_{k=1}^K \mathbf{x}_k$ over the fading channel.

Remark 3. *We note that the proposed beamforming scheme performs well as long as the channel matrices for all nodes are statistically independent, without requiring specific assumptions regarding the distributions of the beamforming matrices. However, isotropic and independent properties help reduce the variance of the error term rapidly. Also, we note that our CSI-unaware fading compensation targets small-scale (fast) fading, which is hard to estimate and varies rapidly. Large-scale factors (pathloss/shadowing) are assumed to be known at the transmitters and handled via power control.*

2) *Correlated Fading Channels*: Due to the isotropic and independent properties of the distribution of the generated \mathbf{V}_k 's, the interference term $\mathbf{y}_{\text{inter}}$ remains zero even in the case that users' channels are correlated, i.e., $\mathbf{H}_{k'}^H \mathbf{H}_k \neq 0$ for all $k, k' \in [K]$. Indeed, in the case where the channel of different nodes are correlated, the massive MIMO system gives us $\mathbf{H}_{k'}^H \mathbf{H}_k \approx N_r \alpha_{k,k'} \mathbf{I}_{N_t}$ where $\alpha_{k,k'}$ is the correlation factor between the channels for users k and k' for $k \neq k'$, and $(k, k') \in [K^2]$. Hence, $\mathbf{y}_{\text{inter}}$ becomes

$$\mathbf{y}_{\text{inter}} = N_r \alpha_{k,k'} \sum_{k,k',k \neq k'}^K \mathbf{V}_{k'}^H \mathbf{V}_k \mathbf{x}_k. \quad (13)$$

Then, invoking the independency property of distribution \mathcal{F}_k from (7), we have $\mathbf{V}_k^H \mathbf{V}_k \approx \mathbf{0}$, which leads to

$$\mathbf{y}_{\text{inter}} \approx N_r \alpha_{k,k'} \mathbf{0} \times \sum_{k=1}^K \mathbf{x}_k = \mathbf{0}. \quad (14)$$

Therefore, employing a large number of antennas at the receiver and transmitter asymptotically diminishes the channel effects.

Remark 4. During the fading compensation, only the CP needs to access the CSI for generating \mathbf{U} from \mathbf{H}_k and \mathbf{V}_k 's. Nodes do not need to communicate their beamforming matrix \mathbf{V}_k every round. Instead, they can share their random seed for generating the matrix \mathbf{V}_k from the distribution \mathcal{F}_k with the CP to avoid the communication overhead for large metrics \mathbf{V}_k 's. In this case, every node only sends a scalar to CP at the beginning of the computation procedure. We emphasize that nodes must generate \mathbf{V}_k i.i.d. according to a specific distribution to ensure statistical fading compensation.

Remark 5. Within the massive MIMO framework, averaging small-scale fading effects yields a more stable sum-channel estimation, rendering it less prone to errors. Specifically, if $\mathbf{H}_k \sim \mathcal{CN}(\mathbf{0}, \sigma_{h,k}^2 \mathbf{I}_{N_r})$ and, under the isotropy condition stated in (6), $\mathbf{U} \sim \mathcal{CN}(\mathbf{0}, \sum_k \sigma_{v,k}^2 \sigma_{h,k}^2 / N_r^2 \mathbf{I}_{N_r})$, where $\sigma_{v,k}^2$ represents the variance of \mathbf{V}_k . Furthermore, because the nodes can compensate for large-scale fading, the distribution simplifies to $\mathbf{U} \sim \mathcal{CN}(\mathbf{0}, K/N_r^2 \mathbf{I}_{N_r})$. Consequently, the receiver beamforming matrix approximates an identity matrix, thereby simplifying its estimation.

Nonetheless, an open question remains: what is the minimum number of receiver antennas required to achieve a desired level of fading error performance? In the next section, we conduct a non-asymptotic analysis to elucidate the relationship between the receiver antenna count and the fading error.

B. How Well Can We Compensate for the Channel Effect?

The previous section discussed the asymptotic elimination of channel effects, including fading and noise, for a sufficiently large number of receiver antennas N_r . Despite this, practical constraints exist on the maximum number of antennas that can be implemented. While including additional antennas improves system capacity, it simultaneously introduces greater complexity. Together with the industry, we must determine an optimal antenna count that adjusts the advantages of increased capacity with the associated complexity.

Therefore, an in-depth examination of how the system capacity fluctuates with the increment in antennas in massive MIMO systems is needed. To this end, we propose a non-asymptotic analysis of the computation error. In the following theorem, we establish a probabilistic upper bound on the MSE.

Theorem 1. Assume a communication network with K nodes equipped with N_t transmitter antennas and the CP with N_r receiver antennas. Let us define the aggregated signal $\mathbf{r} := \sum_{k=1}^K \mathbf{x}_k \in \mathbb{C}^L$, which is generated by the transmitted signal of node k , \mathbf{x}_k , over the fading channel with coefficients $\mathbf{H}_k \sim \mathcal{CN}(\mathbf{0}, N_r \sigma_{h,k}^2 \mathbf{I}_{N_t})$, and beamforming matrices \mathbf{V}_k , which satisfy the isotropy and independency properties

from (6) and (7), respectively, for $k \in [K]$. Also, let us denote by \mathbf{y} the received signal at the CP as in (11). Then, the error norm between the estimated value of $\hat{\mathbf{r}} := \mathbf{y}/\beta$ and \mathbf{r} is upper bounded by ϵ , i.e.,

$$\|\mathbf{r} - \hat{\mathbf{r}}\|_2 \leq \epsilon, \quad (15)$$

in which $N_t \geq L$ and N_r fulfills the lower bound

$$N_r \geq \max \left\{ \frac{2c_{\sigma,\gamma} L K^2 \gamma \sigma_z^2}{\epsilon^2} \ln \left(\frac{2K(L+1)}{\delta} \right), L \right\}, \quad (16)$$

with probability no less than $1 - \delta$, where $\gamma = \sum_{k=1}^K \|\mathbf{x}_k\|_2^2$ represent the transmitter signal power and $c_{\sigma,\gamma} := \min\{\sigma_z^2, \gamma^2\}/16$.

Proof. The proof is provided in Appendix A. \square

The important takeaway from Theorem 1 is that the number of receiver antennas, N_r , has an inverse relation concerning the computation error variance, ϵ^2 , i.e., $N_r = \mathcal{O}(\epsilon^{-2})$. Additionally, the error variance, ϵ^2 , remains unchanged irrespective of the number of nodes, K , in the network. However, maintaining the same error level as the network size increases requires the number of receiver antennas to grow quadratically with K . This quadratic scaling originates from the statistical dependence among the aggregated interference terms in (5b), which limits the effectiveness of averaging and consequently slows down the convergence of the CSI compensation scheme.

We note that the tolerance ϵ is application-driven. We first need to choose ϵ based on the application, (e.g., distributed learning, sensing networks) and then set (N_r, N_t) according to Theorem 1.

Remark 6. Note that the provided analysis in Theorem 1 can be extended for any sub-Gaussian channel noise \mathbf{z} . In the case of heavy-tailed distributions for the channel noise, to mitigate the influence of outliers, we need to consider more advanced techniques, such as M -estimator [41], a Bayesian framework for designing beamforming matrices [42].

While Theorem 1 guarantees $\|\mathbf{r} - \hat{\mathbf{r}}\|_2 \leq \epsilon$ with $N_r = \mathcal{O}(\epsilon^{-2})$, performance degrades when N_r is small—an inherent cost of our CSI-unaware transmitter design. In practice, comparable error targets can be approached with modest arrays by (i) reducing the number of functions L , (ii) averaging across additional time/frequency rounds, and (iii) employing stronger channel coding. If transmitter-side CSI were available (as in CSI-aware OAC [19]), pre-equalization could compensate channel effects and mitigate small-array loss.

C. Imperfect CSI at the Receiver

The proposed framework assumes perfect CSI for beamforming design at the CP. In practice, imperfections in CSI manifest as an additional distortion term in the aggregated signal observed at the CP, which degrades the computation accuracy. To characterize the sensitivity of the proposed scheme to CSI uncertainty, we model the imperfect CSI using channel estimation error model from [43]. In particular, for node k , the estimated channel matrix is modeled as

$$\hat{\mathbf{H}}_k = \mathbf{H}_k + \Delta \mathbf{H}_k, \quad (17)$$

where \mathbf{H}_k denotes the true channel realization and $\Delta\mathbf{H}_k$ represents the estimation error, assumed to be statistically independent of \mathbf{H}_k . The estimation error is usually modeled as $\Delta\mathbf{H}_k$, whose i.i.d. entries distributed as $\mathcal{CN}(0, \sigma_{I,k}^2)$. Given this model, the CP selects $\mathbf{U} = \sum_{k=1}^K \mathbf{V}_k^H \hat{\mathbf{H}}_k^H / N_r$. Under imperfect CSI, the received signal can be decomposed as $\tilde{\mathbf{y}} = \mathbf{y} + \Delta\mathbf{y}$, where \mathbf{y} corresponds to the perfect CSI aggregation in (4) and $\Delta\mathbf{y}$ captures the distortion induced by channel estimation errors. This distortion term is given by

$$\Delta\mathbf{y} = \frac{1}{\beta} \sum_{k,k'=1}^K \mathbf{V}_{k'}^H \Delta\mathbf{H}_{k'}^H \mathbf{H}_k \mathbf{V}_k \mathbf{x}_k + \frac{1}{\beta} \sum_{k=1}^K \mathbf{V}_k^H \Delta\mathbf{H}_k^H \mathbf{z}. \quad (18)$$

Due to the statistical independence between all \mathbf{H}_k , $\Delta\mathbf{H}_k$, and the noise vector \mathbf{z} [44], and leveraging the channel hardening property, the distortion term vanishes asymptotically as the number of receive antennas grows. In particular, we have $\lim_{N_r \rightarrow \infty} \Delta\mathbf{y} = \mathbf{0}$, which consequently give us $\lim_{N_r \rightarrow \infty} \tilde{\mathbf{y}} = \mathbf{y} = \sum_{k=1}^K \mathbf{x}_k$. Hence, imperfect CSI does not induce a persistent bias in the large-antenna regime. In other words, $\Delta\mathbf{y}$ effectively behaves as an additional interference or noise component. Defining $\tilde{\mathbf{z}} := \mathbf{z} + \Delta\mathbf{y}$, its variance $\sigma_{\tilde{\mathbf{z}}}^2$ scales as $\sigma_z^2 + \sum_k \sigma_{I,k}^2$. Incorporating this effect leads to the following Theorem .

Theorem 2. *Under the same conditions as Theorem 1, and considering imperfect CSI at the receiver modeled by $\Delta\mathbf{H}_k$ whose i.i.d. entries distributed as $\mathcal{CN}(0, \sigma_{I,k}^2)$ for $k \in [K]$, the computation error bound in (15) holds provided that $N_r, N_t \geq L$ and N_r satisfies*

$$N_r \geq 8 \frac{c_{\sigma,\gamma} L K^2 \gamma \sigma_z^2 \max\{\bar{\xi}, 1\}}{\epsilon^2} \ln\left(\frac{4K(L+1)}{\delta}\right). \quad (19)$$

with probability at least $1 - \delta$, where $\bar{\xi} = \sum_k \sigma_{I,k}^2 \sigma_{h,k}^{-2} / K$.

Proof. The proof is provided in Appendix F. \square

Theorem 2 indicates that, as long as $\bar{\xi} \leq 1$, the presence of channel estimation errors does not increase the required number of receive antennas compared with the perfect CSI case. Equivalently, no additional antennas are needed to achieve the same aggregation accuracy. The condition $\bar{\xi} = 1$ corresponds to a normalized estimation error power on the order of the channel power, i.e., $\sigma_{I,k}^2 / \sigma_{h,k}^2 \approx 1$. In practical systems, channel estimation errors are typically well below this level (often within approximately 20% [43]), which indicates that the proposed VecComp scheme is robust to CSI imperfections at the receiver.

IV. VECOMP FOR MULTIPLE FUNCTION COMPUTATION

So far, we have designed beamforming matrices to compensate for the effect of the channel in performing function computation. In this section, we introduce the VecComp approach for computing matrix functions by designing the encoders \mathcal{E}_k s and decoder \mathcal{T} . VecComp has two distinct setups:

- **Exact Setup:** the channel effects are entirely compensated through the beamforming technique outlined in the previous section.
- **Inexact Setup:** the received signal is contaminated with a certain error tolerance, e.g., $\eta > 0$.

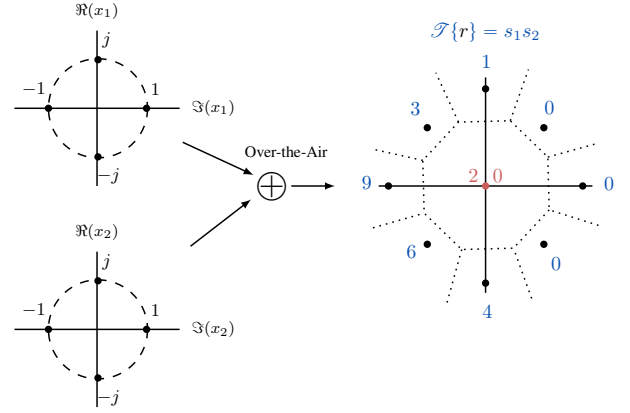


Figure 2. The overlaps of the reshaped constellation points of QPSK modulation do not allow us to compute the product function.

A. VecComp: Function Computation in Exact Setup

In the exact setup, we assume that the received signal by the CP is error-free, i.e., $\mathbf{r} := \sum_{k=1}^K \mathbf{x}_k$. The CP applies the tabular function $\mathcal{T} : \mathbb{C}^L \mapsto \mathbb{R}^L$ on the induced signal \mathbf{r} to compute the desired function $\mathbf{f}(\mathbf{s}) \in \mathbb{R}^L$ function, i.e.,

$$\mathcal{T}\left(\sum_{k=1}^K \mathcal{E}_k(s_k)\right) \approx \mathbf{f}(\mathbf{s}), \quad (20)$$

where $\mathcal{E}_k(s_k) := [\mathcal{E}_{k,1}(s_k), \dots, \mathcal{E}_{k,L}(s_k)]^T$. Because the encoding operator $\mathcal{E}_k(s_k)$ acts element-wise on the input scalar s_k , we decompose the tabular function \mathcal{T} into a sets of L different maps as $\mathcal{T}(\mathbf{r}) = \bigoplus_{\ell=1}^L \mathcal{T}_\ell(r_\ell)$, in which, every $\mathcal{T}_\ell : \mathbb{C} \mapsto \mathbb{R}$ maps the element ℓ of received vector \mathbf{y}_ℓ to output ℓ of function $\mathbf{f}(\mathbf{s})$ as

$$\mathcal{T}_\ell\left(\sum_{k=1}^K \mathcal{E}_{k,\ell}(s_k)\right) = f_\ell(s_1, \dots, s_K). \quad (21)$$

We must guarantee that the employed encoders $\mathcal{E}_{k,\ell}$ and tabular functions \mathcal{T}_ℓ for nodes can accurately compute the desired function to hold the equality in (21). Figure 2 shows a simple case for $K = 2$ nodes that want to compute the product function $f(s_1, s_2) = s_1 s_2$ with $L = 1$. The constellation points shaped by the nodes cannot be uniquely mapped to the product function. Indeed, the induced constellation diagram of $\sum_{k=1}^K \mathcal{E}_{k,\ell}(s_k)$ must cover all the points in the range of function $\mathbf{f}(\mathbf{s})$ [6]. In other words, for any distinct value in the range of function $\mathbf{f}(\mathbf{s})$, there must exist a corresponding distinct constellation point in the diagram of $\sum_{k=1}^K \mathcal{E}_{k,\ell}(s_k)$. This condition can be expressed in the following proposition.

Proposition 1. *For $\ell \in [L]$, let $f_\ell^{(i)}$ be the i -th output of the function f_ℓ for given values of input $s_1^{(i)}, s_2^{(i)}, \dots, s_K^{(i)} \in \mathbb{F}_Q^K$ from $i \in [M]$, where M denotes the number of possible values of the function f_ℓ . Further, $r_\ell^{(i)} \in \mathbb{C}$ represents the corresponding constellation points to $f_\ell^{(i)}$, i.e., $r_\ell^{(i)} = \sum_{k=1}^K \mathcal{E}_{k,\ell}(s_k^{(i)})$. Then, using the set of encoders $\mathcal{E}_{k,\ell}(\cdot)$ and the tabular functions $\mathcal{T}_\ell(\cdot)$ for $\ell \in [L]$, the computation in (21) is correctly performed over the MAC if and only if we have the following:*

$$\text{if } f_\ell^{(i)} \neq f_\ell^{(j)} \text{ then } r_\ell^{(i)} \neq r_\ell^{(j)}, \quad \forall (i, j) \in [M]^2. \quad (22)$$

Given feasibility of the computation over the MAC, there exists a map $\mathcal{T} = \bigoplus_{\ell=1}^L \mathcal{T}_\ell$ such that $\mathcal{T}\left(\sum_{k=1}^K \mathcal{E}_k(s_k)\right) = \mathbf{f}(s)$, i.e., the desired function f can be correctly computed.

Proof. Let us consider $f_\ell^{(i)} = f_\ell^{(j)} = d_\ell$. Then, regardless of the values $r_\ell^{(i)}$ and $r_\ell^{(j)}$, we can define a tabular map \mathcal{T}_ℓ such that $\mathcal{T}_\ell(r_\ell^{(i)}) = \mathcal{T}_\ell(r_\ell^{(j)}) = d_\ell$. Therefore, this shows that we need distinct constellation points only for distinct output values of the function f_ℓ as stated in the theorem. \square

The induced diagram of the constellation point i at antenna ℓ in terms of the transmitted modulation vectors of the nodes can be expressed as

$$r_\ell^{(i)} = \langle \mathbf{a}_{\ell,i}, \mathbf{X}_\ell \rangle, \quad (23)$$

where $\mathbf{X}_\ell := [\mathbf{X}_{\ell,1}, \dots, \mathbf{X}_{\ell,K}]^\top \in \mathbb{C}^{QK}$ whose $[\mathbf{X}_{\ell,k}]_q = x_{k,\ell}^q$ denotes q -th elements of the constellation points owned by node k at antenna ℓ , for $(q, k) \in [Q] \times [K]$. Also, $\mathbf{a}_{\ell,i}$ is a binary vector whose elements are determined such that it selects all the constellation points corresponding to function value $f_\ell^{(i)}$.

Based on the Proposition 1, to have a valid computation over the MAC for the desired function $\mathbf{f}(s) : \mathbb{F}_Q^K \mapsto \mathbb{R}^L$, we pose the following optimization problem

$$\begin{aligned} \mathcal{P}_\ell^{(1)} = & \text{find } \mathbf{X}_\ell \\ \text{s.t. } & r_\ell^{(i)} \neq r_\ell^{(j)}, \forall (i, j) \in \Omega, \|\mathbf{X}_\ell\|_{\mathbb{F}}^2 \leq 1, \end{aligned} \quad (24)$$

where $\Omega \subseteq [M^2]$ whose every element (i, j) is selected as $f_\ell^{(i)} \neq f_\ell^{(j)}$, and P is the allocated power to all node's modulation vectors. For the constraints in (24) on valid computation, we use the given notation in (23) as

$$\begin{aligned} \langle \mathbf{a}_{\ell,i}, \mathbf{X}_\ell \rangle & \neq \langle \mathbf{a}_{\ell,j}, \mathbf{X}_\ell \rangle, \\ \langle \mathbf{a}_{\ell,i} - \mathbf{a}_{\ell,j}, \mathbf{X}_\ell \rangle & \neq 0, \\ \langle \boldsymbol{\alpha}_\ell^{i,j}, \mathbf{X}_\ell \rangle & \neq 0, \quad \forall (i, j) \in \Omega. \end{aligned} \quad (25)$$

The last not equal term can be equivalently written as $\mathbf{X}_\ell \perp \boldsymbol{\alpha}_\ell^{i,j}$ for $(i, j) \in \Omega$. Let us define set $\mathcal{A}_\ell^\Omega := \{\boldsymbol{\alpha}_\ell^{i,j}, (i, j) \in \Omega\}$, which involves all vectors $\boldsymbol{\alpha}_\ell^{i,j}$. Then, Problem $\mathcal{P}_\ell^{\text{exact}}$ can be equivalently written as

$$\begin{aligned} \mathcal{P}_\ell^{(1)} = & \text{find } \mathbf{X}_\ell \\ \text{s.t. } & \langle \tilde{\boldsymbol{\alpha}}_\ell, \mathbf{X}_\ell \rangle \neq 0, \forall \tilde{\boldsymbol{\alpha}}_\ell \in \mathcal{A}_\ell^\Omega, \|\mathbf{X}_\ell\|_{\mathbb{F}}^2 \leq 1. \end{aligned} \quad (26)$$

Problem $\mathcal{P}_\ell^{\text{exact}}$ is a feasibility problem to find a point that satisfies the constraints, and the solution is not unique. Indeed, $\mathcal{P}_\ell^{\text{exact}}$ finds a vector not perpendicular to a given set of vectors in \mathcal{A}_ℓ^Ω . One possible way to obtain a solution for Problem $\mathcal{P}_\ell^{\text{exact}}$ is given by Algorithm 1. The following proposition guarantees the feasibility of Algorithm 1.

Proposition 2. Let $\hat{\mathbf{Y}}_\ell = \text{NonOrth}(\mathcal{A}_\ell^\Omega) \in \mathbb{C}^{QK}$ be the output from Algorithm 1. Then, $\hat{\mathbf{X}}_\ell = (\hat{\mathbf{Y}}_\ell + \tilde{\mathbf{X}}_\ell)/\kappa$, where $\kappa = \sqrt{\|\hat{\mathbf{Y}}_\ell\|_2^2 + \|\tilde{\mathbf{X}}_\ell\|_2^2}$ and $\tilde{\mathbf{X}}_\ell \in \mathcal{N}(\mathcal{A}_\ell^\Omega)$, is a solution to Problem $\mathcal{P}_\ell^{\text{exact}}$.

Proof. See Appendix B. \square

Given the proposed solution in Proposition 2, we can design the encoders as nonlinear operators that map the input value s

Algorithm 1 Find non-orthogonal vector

- 1: **procedure** NonOrth($\mathbf{v}_1, \dots, \mathbf{v}_m$)
 - 2: Reorder vectors such that $\{\mathbf{v}_2, \dots, \mathbf{v}_k\} \perp \mathbf{v}_1$ are orthogonal and $\{\mathbf{v}_{k+1}, \dots, \mathbf{v}_m\} \not\perp \mathbf{v}_1$ are not
 - 3: Recursively, $\mathbf{y} := \text{NonOrth}(\mathbf{v}_2, \dots, \mathbf{v}_k)$.
 - 4: $\alpha = \max \left\{ \left| \frac{\langle \mathbf{y}, \mathbf{v}_i \rangle}{\langle \mathbf{v}_1, \mathbf{v}_i \rangle} \right| : i \in \{k+1, \dots, m\} \right\} + 1$.
 - 5: $\mathbf{x} \leftarrow \alpha \mathbf{v}_1 + \mathbf{y}$
 - return** x
 - 6: **end procedure**
-

to the set of the obtained constellation points. In particular, we define set \mathcal{S}_k involving all possible values of $s_k \in \mathbb{F}_Q$, and \mathcal{X}_k involves all the values of column k of $\hat{\mathbf{X}}_\ell$ for $\ell \in [L]$. Then, \mathcal{E}_k becomes the bijective function that maps the elements of \mathcal{S}_k to the elements of set \mathcal{X}_k , i.e., $\mathcal{E}_k : \mathcal{S}_k \mapsto \mathcal{X}_k$ and

$$\hat{\mathcal{E}}_{k,\ell} = s_k^{(q)} \mapsto \hat{x}_{k,\ell}^{(q)}, \quad \forall (\ell, q) \in [L] \times [Q]. \quad (27)$$

Similarly, having access to the encoders, the tabular function \mathcal{T} can be determined uniquely. Indeed, we define set $\mathcal{X} := \bigoplus_{k=1}^K \mathcal{X}_k$, and define \mathcal{W}_ℓ^f as the range of function $f_\ell(s)$ for $\ell \in [L]$. Then, the tabular function $\mathcal{T}_\ell(\cdot) : \mathcal{X} \mapsto \mathcal{W}_\ell^f$ is determined as the map

$$\hat{\mathcal{T}}_\ell = \sum_{k=1}^K \hat{x}_{k,\ell}^{(q)} \mapsto f_\ell(s_1^{(q)}, \dots, s_K^{(q)}), \quad \forall \ell \in [L]. \quad (28)$$

Consequently, we get $\hat{\mathcal{T}} := \bigoplus_{\ell=1}^L \hat{\mathcal{T}}_\ell$.

Remark 7. So far, we have provided a mechanism to compute a multivariate function $\mathbf{f}(s) \in \mathbb{R}^L$ in a distributed manner for a network consisting of K nodes and the CP server, i.e., $\mathcal{T}\left(\sum_{k=1}^K \mathcal{E}_k(s_k)\right) = \mathbf{f}(s)$. Giving the desired function $\mathbf{f}(s)$, the CP compute the modulation constellations $\hat{\mathbf{X}}_\ell$ from Proposition 2. Then, the CP shares the encoder $\mathcal{E}_k(\cdot)$ to node k for $k \in [K]$. Subsequently, node k build the encoder \mathcal{E}_k and employs its modulation vector \mathbf{x}_k for computing the function $\mathbf{f}(s)$.

B. VecComp: Function Computation for Inexact Setup

Let e be the uncompensated error over the MAC, the CP receives $\tilde{\mathbf{r}} := \mathbf{r} + e$ where $\|e\|_2 \leq \eta$. For $\eta > 0$, solutions to Problem $\mathcal{P}_\ell^{\text{exact}}$ may result in high computation error even for a small value of η . To ensure the robustness of the solution to the error, we need to modify the constraints for Problem $\mathcal{P}_\ell^{\text{exact}}$ in (26) to capture the computation errors.

Indeed, the angle between \mathbf{X}_ℓ and vectors $\boldsymbol{\alpha}_\ell^{i,j}$ for $(i, j) \in \Omega$ must be dependent on the value of the corresponding computation error, i.e., $|f_\ell^{(i)} - f_\ell^{(j)}|$. Accordingly, we replace them with a smoother condition, such as:

$$\begin{aligned} \mathcal{P}_\ell^{(1)} = & \max_{\mathcal{E} > 0, \mathbf{X}_\ell} \mathcal{E} \\ \text{s.t. } & \langle \boldsymbol{\alpha}_\ell^{i,j}, \mathbf{X}_\ell \rangle^2 \geq \mathcal{E} \gamma_{i,j}^\ell, \quad \|\mathbf{X}_\ell\|_{\mathbb{F}}^2 \leq 1, \end{aligned} \quad (29)$$

for all $(i, j) \in \Omega$, where $\gamma_{i,j}^\ell := |f_\ell^{(i)} - f_\ell^{(j)}|^2$ penalize the distance between zero with different weight proportional to the computation error $|f_\ell^{(i)} - f_\ell^{(j)}|$. Problem $\mathcal{P}_\ell^{(1)}$ is a quadratically constrained quadratic programming (QCQP) problem with

Algorithm 2 Design the Modulation Vectors

```

1: Input: Function  $\mathbf{f}(s_1, \dots, s_K)$ 
2: Set  $M = Q^K$ 
3: Output: Modulation vectors  $\{\mathbf{X}_\ell\}_{\ell=1}^L$ 
4: procedure OPTIMIZATION( $\{f_\ell^{(i)}\}_{(i,\ell)=(1,1)}^{[M] \times [L]}$ )
5:   for in parallel  $\ell \leftarrow 1, 2, \dots, L$  do
6:     Obtain  $\mathbf{W}_\ell$  by solving (30)
7:     Cholesky decomposition for  $\mathbf{W}_\ell = \mathbf{L}_\ell \mathbf{L}_\ell^H$ 
8:     Set  $\mathbf{X}_\ell = \mathbf{L}_\ell$ 
9:   end for
10: end procedure

```

non-convex constraints, and it is known to be *NP-hard* [45]. To circumvent the non-convexity, we use the *lifting trick* by treating $\mathbf{X}_\ell \mathbf{X}_\ell^T$ as matrix \mathbf{W}_ℓ for $\ell \in [L]$. Then, following a similar strategy as [6], we can reach the following relaxed convex optimization problem,

$$\begin{aligned} \mathcal{P}_\ell^{(2)} = \max_{\mathcal{E} > 0, \mathbf{W}_\ell} \mathcal{E} \quad \text{s.t.} \quad & \langle \mathbf{B}_\ell^{i,j}, \text{trace}(\mathbf{W}_\ell) \rangle \geq \mathcal{E}, \\ & \text{trace}(\mathbf{W}_\ell) \leq 1, \mathbf{W}_\ell \geq \mathbf{0}. \end{aligned} \quad (30a)$$

The optimization problem denoted as $\mathcal{P}_\ell^{(2)}$ is formulated as a semi-definite programming (SDP) problem. By solving this problem, we obtain the optimal weight matrix \mathbf{W}_ℓ^* . Subsequently, the optimal solution \mathbf{X}_ℓ^* is computed through the Cholesky factorization of \mathbf{W}_ℓ^* [46], specifically when \mathbf{W}_ℓ^* resulted in a rank-one matrix. In instances where \mathbf{W}_ℓ^* is not a rank-one matrix, a sub-optimal solution for $\mathcal{P}_\ell^{(1)}$ is retrievable via Gaussian randomization techniques [46]. The overall procedure is summarized in Algorithm 2.

It is worth noting that the modulation design in (30) extends directly to the T -retransmission (time-slot) setting in Remark 3. Concretely, replace \mathbf{W}_ℓ^* by its best rank- T approximation $\mathbf{W}_\ell^{(T)}$ (e.g., retain the top T eigenvalues/vectors of \mathbf{W}_ℓ^*), and factorize $\mathbf{W}_\ell^{(T)}$ to obtain the T -slot encoder. This construction is optimal for the T -slot design objective [47] and improves reliability through retransmissions, thereby enabling a controllable reliability–latency tradeoff [47].

Remark 8. *Optimal solutions to each instance of Problem $\mathcal{P}_\ell^{(1)}$, where $\ell \in [L]$, enable the computation of the desired function $\mathbf{f}(\mathbf{s})$ over the fading MAC. Upon attaining \mathbf{X}_ℓ^* , the encoders \mathcal{E}_k are systematically constructed for all K nodes, following the methodology outlined in Eq. (27). For the decoding sets \mathcal{T}_ℓ , a Voronoi diagram is generated based on the complete set of feasible constellation points, employing a maximum likelihood estimator [6], [48]. Subsequently, decoder \mathcal{T}_ℓ is defined as a tabular function mapping points within the resultant Voronoi cells to the corresponding output of $f_\ell(\mathbf{s})$, for each $\ell \in [L]$.*

Remark 9. *VecComp raises ChannelComp’s complexity only linearly in the number of functions, L . Since ChannelComp’s SDP solver runs in $\mathcal{O}(\max\{n, m\}^4 n^{0.5})$ [6], VecComp’s overall complexity becomes $\mathcal{O}(L \max\{n, m\}^4 n^{0.5})$, with decoding scaling as $\mathcal{O}(LQ')$. All other metrics—spectral efficiency and per-transmission energy—remain identical to ChannelComp,*

with the only extra cost due to standard Massive MIMO multi-antenna reception [49].

Remark 10. *In VecComp, increasing the number of nodes K raises both optimization complexity and antenna requirements. For instance, sum-function constraints grow as $\mathcal{O}(K^2)$ in (30), enabling more complex computations at the cost of heavier optimization. Meanwhile, (16) shows the receiver antennas must scale as $N_r = \mathcal{O}(LK/\epsilon^2)$ to preserve error tolerance ϵ . Thus, designers must trade off node count against available antennas to balance efficiency and reliability.*

V. APPLICATION CONTEXT: DISTRIBUTED ML AND IOT

VecComp provides a digital modulation framework for computing vector functions directly over the wireless MAC. This capability is particularly relevant in distributed machine learning and IoT systems, where uplink communication constitutes a critical bottleneck [50]. Instead of transmitting raw data, each device k encodes its local task vector \mathbf{s}_k —originating from learning or sensing pipelines—into channel symbols. The receiver, equipped with CSI, can then form one-shot linear estimates $f(\mathbf{x})$ of the desired function while remaining compatible with conventional channel coding, quantization, and MIMO techniques.

This paradigm reduces uplink traffic, scales efficiently with the number of devices, and naturally supports computational primitives that frequently arise in ML/IoT applications. Typical examples of the desired function include aggregation, affine transformations, and short-window convolutions. To illustrate, the subsequent subsections instantiate VecComp for two representative cases: (i) affine transformations implemented via PAM (Sec. V-A), and (ii) convolution operations realized via QAM (Sec. V-B).

A. Special Case I: Affine Transformation with PAM

One appropriate computation is to use an affine transformation, in which an affine map comprises two functions: a translation and a linear map. This can be useful in applications such as wireless sensor networks and edge computing, in which computations are typically limited to affine transformation (weighted summation) [51]. Mathematically, an affine transform can be represented by:

$$\mathbf{y} = \mathbf{f}(\mathbf{s}) = \mathbf{A}\mathbf{s} + \mathbf{b}, \quad \mathbf{s} \in \mathbb{F}_Q^K, \quad (31)$$

where $\mathbf{A} \in \mathbb{F}_{Q'}^{L \times K}$ represents a linear map with $Q' := \prod_{k=1}^K Q_k$, and $\mathbf{b} \in \mathbb{F}_Q^L$ is the translation function. We can rewrite the transformation as follows:

$$f_\ell(s_1, \dots, s_K) = \sum_{k=1}^K a_{k,\ell} s_k + b_\ell, \quad \ell \in [L], \quad (32)$$

where $a_{k,\ell} \in \mathbb{F}_{Q_K}$ denotes the entry of matrix \mathbf{A} at (ℓ, k) , b_ℓ is element ℓ of vector \mathbf{b} . For ease of explanation, consider the field \mathbb{F} to be an integer field \mathbb{Z} , i.e., $\mathbb{F}_{Q_k} = \mathbb{Z}_{Q_k} := \{0, 1, \dots, Q_k - 1\}$ for $k \in [K]$. Then, the product $a_{k,\ell} s$ belongs to \mathbb{F}_{Q_k} field, and we can use the following encoder for transmission:

$$\mathcal{E}_{k,\ell}(s) = a_{k,\ell} s - \left\lfloor \frac{Q_k}{2} \right\rfloor, \quad (\ell, k) \in [L] \times [K], \quad (33)$$

in which \mathcal{E}_k maps the input value onto the constellation point of a pulse-amplitude modulation (PAM). Having encoders \mathcal{E}_k 's, the decoder accordingly becomes:

$$\mathcal{T}_\ell(y) = D(y) + b_\ell + \sum_{k=1}^K \left\lfloor \frac{Q Q_k}{2} \right\rfloor, \quad \ell \in [L], \quad (34)$$

where

$$D(y) = \begin{cases} r, & r - 0.5 \leq y \leq r + 0.5, \in r \in \mathbb{Z}_{Q_f}, \\ (1 - Q) \sum_{k=1}^K (1 - Q_k), & y < K(1 - Q) + 0.5, \\ \sum_{k=1}^K (Q_k - 1)(Q - 1), & y > \varsigma - 0.5, \end{cases}$$

where $\varsigma = \sum_{k=1}^K (Q_k - 1)(Q - 1)$. Notably, we observe that the proposed \mathcal{E}_k in (33) satisfies all the constraints in (29). Therefore, from Proposition 1, we know that $\mathcal{T}_\ell \left(\sum_{k=1}^K \mathcal{E}_{k,\ell}(s_k) \right) = f_\ell(s_1, \dots, s_K)$ holds over ideal MAC.

B. Special Case II: Convolution with QAM

VecComp offers an innovative approach to convolution operations, a cornerstone in convolutional neural networks (CNNs). Traditionally, CNNs have been implemented using over-the-air analog computation, as explored in [52], where the convolution operation is achieved through reconfigurable intelligent surfaces. Contrary to this analog-based method, VecComp facilitates convolution operations via digital computing. This approach negates the need for complex reconfiguration and transition to analog systems, presenting a more straightforward, digital-centric solution for executing convolution operations in CNNs. More precisely, for a given vector $\mathbf{a} \in \mathbb{F}_Q^{L+K-1}$, the convolution operator of \mathbf{a} and nodes' data \mathbf{s} of size $K \times 1$ can be written as

$$\mathbf{f}(\mathbf{s}) = \mathcal{H}(\mathbf{a})\mathbf{s}, \quad (35)$$

where $\mathcal{H}(\mathbf{a})$ with size of $L \times K$ indicates the Hankel transform of vector \mathbf{a} with matrix pencil parameter K [53]. Then, the element-wise formula is given by

$$f_\ell(s_1, \dots, s_K) = \sum_{k=1}^K a_{\ell-1+k} s_k, \quad \ell \in [L]. \quad (36)$$

To compute the given function using QAM, we can solve the optimization problem in (30) to obtain the optimal modulation vector. However, one can use a closed-form formula proposed in [7, Section III] as a solution to (30). For \mathbb{F} equals to \mathbb{Z} , node k can encode $a_{\ell-1+k} s_k$ into in-phase and quadrature components of digital modulation as follows:

$$\mathcal{E}_{k,\ell}(s) := a_{\ell-1+k} s - Q \cdot \left\lfloor \frac{a_{\ell-1+k} s}{Q} \right\rfloor + \frac{1-Q}{2} + j \left(\left\lfloor \frac{a_{\ell-1+k} s}{Q} \right\rfloor + \frac{1-Q}{2} \right), \quad (37)$$

in which \mathcal{E}_k maps the input value onto the constellation points of a quadrature amplitude modulation (QAM) of order Q^2 . Having encoders \mathcal{E}_k 's, the decoder accordingly becomes:

$$\mathcal{T}_\ell(y) = \mathcal{W}(\Re(y)) + Q \cdot \left(\mathcal{W}(\Im(y)) + \frac{Q-1}{2} \right) + \frac{Q-1}{2},$$

where $\mathcal{W}(\cdot)$ is the round up to half function, i.e., $\mathcal{W}(z) = \lceil z + 0.5 \rceil - 0.5$. VecComp's QAM-based modulation encoders can accelerate computer applications, particularly in scenarios

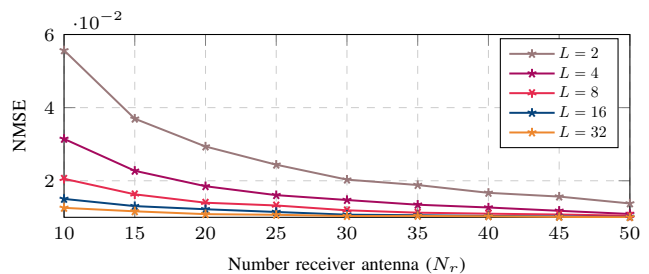


Figure 3. NMSE performance of VecComp as a function of the number of receiver antennas, N_r , for varying computation dimensions L . The setup assumes $N_t = L$ and SNR = 20, dB, with simulation results averaged over 10^3 Monte Carlo trials. The figure illustrates the improvement in computation robustness and fading resilience as N_r increases from 10 to 50, highlighting the effect of antenna scaling on VecComp's ability to accurately compute the sum function in a fading environment.

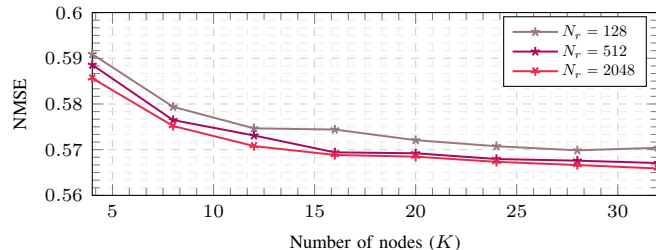


Figure 4. NMSE performance of VecComp as a function of the number of transmitting nodes, K , for different receiver antenna configurations. The simulation is conducted with $N_t = 4$, $L = 4$, and SNR = 5 dB, with results averaged over 10^4 Monte Carlo trials.

where vector-based computations are needed for convolutional operations.

Remark 11. *The given encoders in subsections V-A and V-B particularly work only for affine and convolution functions with corresponding modulations, respectively. For general function computation, $\mathcal{P}_\ell^{\text{inexact}}$ may not have a closed-form solution, and to perform the computation, we need to follow the procedure in Algorithm 2.*

In the following section, we assess the performance of the proposed VecComp method for computation matrix function over the fading MAC.

VI. NUMERICAL EXPERIMENTS

We divide this section into three parts to evaluate VecComp's performance for fading compensation and vector computation tasks for different numbers of nodes, antennas, and noise levels. In the first part, we analyze the performance of the proposed beamforming technique to compensate for the fading effect. Next, we analyze VecComp's performance for computing various functions with multiple orders of modulations and several nodes over the noisy MAC. Finally, we evaluate the computation performance over different noise levels. In particular, we compare the performance of VecComp on the following three settings: 1) an analog MIMO approach [19] in which the sum function is computed over the air, while general functions are obtained via nomographic approximation. 2) a conventional digital MIMO transmission scheme based on

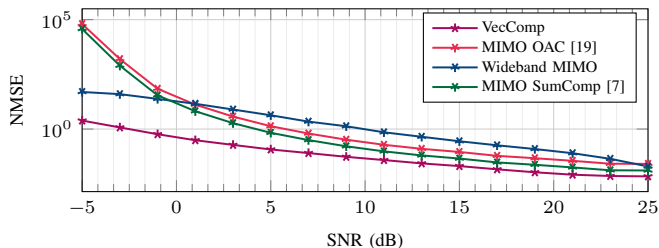


Figure 5. Performance comparison between VecComp, MIMO OAC [19], MIMO SumComp [7], and wide-band MIMO in terms of NMSE error averaged over $N_s = 100$, where input values are given by $x_k = \{0, 1, \dots, 7\}$ and the desired functions are $f_1 = \prod_k x_k$, $f_2 = \sum_k x_k/K$, $f_3 = \max_k x_k$, and $f_4 = \sum_k x_k^2$.

orthogonal frequency-division multiple access, where nodes occupy distinct frequency subchannels and multiple function outputs are supported through MIMO processing; and 3) the digital SumComp scheme [7], which is extended in this work to a MIMO setup for the simulations and follows a structure similar to the analog MIMO approach but employs digital QAM modulation for sum computation and nomographic approximation for general functions. To maintain focus on VecComp’s primary objective, which is achieving reliable vector computation in fading environments, we mainly concentrate on function computation and channel compensation within the VecComp framework.

A. Number of Antennas

In this subsection, we explore how the number of antennas impacts VecComp’s ability to compensate for fading effects and accurately compute the sum function. The nodes compute the sum function over fading MAC, where channel coefficients are generated randomly according to the Gaussian distribution, i.e., $\mathbf{H}_k \sim \mathcal{CN}(\mathbf{0}, N_r \sigma_h^2 \mathbf{I}_{N_t})$ with $\sigma_h^2 = 1$. For beamforming vectors, we generated them by $\mathbf{V}_k \sim \mathcal{CN}(\mathbf{0}, \mathbf{I}_L)$ to ensure that they satisfy the isotropic properties. We also consider scenarios where the number of nodes $K = 100$, the number of transmitter antennas $N_t = L$, and the number of receiver antennas varies, studying configurations ranging from $N_r = 10$ to $N_r = 50$ to determine the effect of antenna scaling on normalized MSE (NMSE) performance. The simulation results averaged over 10^3 Monte Carlo trials with signal-to-noise ratios (SNRs) equal to 20 dB. Figure 3 illustrates how the increase in receiver antenna N_r , from 10 to 50, improves computation robustness and fading resilience across various function computation L . Moreover, the increased number of functions for computation L leads to lower NMSE. In particular, by increasing the number of antennas from $N_r = 10$ to $N_r = 50$, we observe around 75% reduction of NMSE.

B. Number of Nodes

In this subsection, we assess the effect of varying the number of transmitting nodes on the performance of VecComp. The experiment considers a variable number of nodes, K , ranging from 4 to 32 in increments of 4, while fixing the number of transmitter antennas at $N_t = 4$ and the beamforming

dimension at $L = 4$. Consistent with the previous analysis, channel matrices are generated as $\mathbf{H}_k \sim \mathcal{CN}(\mathbf{0}, N_r \sigma_h^2 \mathbf{I}_{N_t})$ with $\sigma_h^2 = 1$, and beamforming matrices are drawn from $\mathbf{V}_k \sim \mathcal{CN}(\mathbf{0}, \mathbf{I}_L)$, normalized to satisfy the power constraints. The combined received signal, resulting from the superposition of contributions from all nodes and subject to additive noise, is processed to yield the NMSE as the performance metric.

Figure 4 illustrates that the NMSE remains approximately constant as K increases, which is consistent with the prior experiment where increasing the number of antennas reduced the overall error. Although the MSE increases with the number of nodes—owing to the higher aggregate power in $\|\sum_k \mathbf{x}_k\|$ —this effect is counterbalanced by the corresponding increase in the norm of the sum of transmitted symbols as elucidated by Remark 10. Consequently, the NMSE, defined as the MSE normalized by $\|\sum_k \mathbf{x}_k\|^2$, remains invariant to K . This result underscores the robustness of the VecComp scheme in accommodating a massive number of nodes.

C. Complex Modulations

We assess the impact of VecComp’s designed modulation on the aggregated function computation performance over the noisy MAC compared to the following methods: 1) analog MIMO scheme [19], where nodes use analog modulation for transmission, 2) wideband MIMO scheme, where each node transmits over a distinct communication channel and uses multiple antennas to compute multiple functions at the CP, and 3) digital MIMO scheme [7], termed SumComp, where nodes use QAM style modulation for transmission and computing sum function over the MAC. Note that we are only comparing the computation aspect of the mentioned scheme here, as there is no fading. Four distinct functions, $L = 4$, are considered: the product, mean, maximum, and sum-of-squares, each realized via a dedicated modulation vector obtained from (30). The NMSE is computed over a range of SNR values from -5 dB to 25 dB.

Figure 5 illustrates the NMSE performance for the three methods as a function of SNR. The results demonstrate that, as the SNR increases, the aggregated NMSE decays monotonically. Moreover, VecComp shows superior performance thanks to the designed modulation for each desired function, which improved around 10 dB in NMSE in low SNR areas. Furthermore, the analog MIMO scheme cannot accurately compute the maximum function, even in low SNR scenarios, due to its approximation techniques for computing the maximum and product functions.

D. Computational Complexity of the Design

To complement the performance results, we provide the computational complexity of VecComp, MIMO SumComp [7], and a naïve L -dimensional extension based on Remark 9, both relative to ChannelComp. Figure 6 depicts the ratios of the SDP solving cost and decoding cost with respect to ChannelComp when $L = 1$, while varying the order of modulation q , the number of nodes K , and the vector length L . The results show that the complexity of VecComp grows only linearly in L , leading to a constant ratio (equal to L) when compared

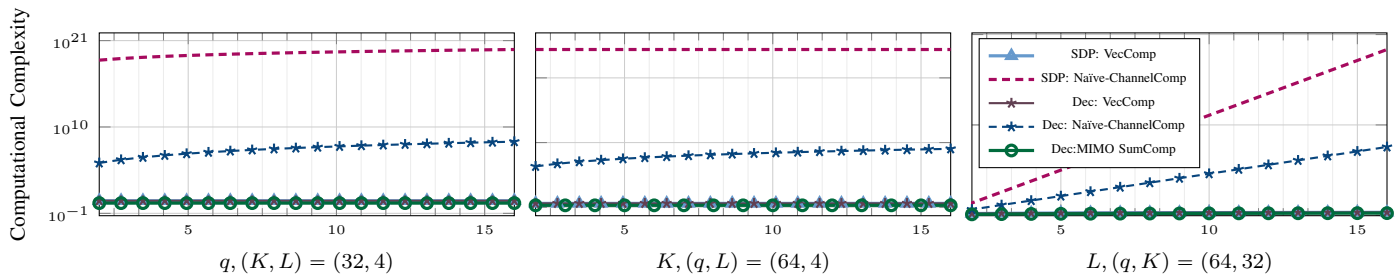


Figure 6. Computational complexity comparison of VecComp, MIMO SumComp, and a naïve L -dimensional extension of ChannelComp. The figure depicts the ratio of the complexities, both for solving the SDP in the modulation design and for the decoding procedure, relative to ChannelComp. Subplots from left to right vary with modulation order q , number of nodes K , and vector length L , respectively. The logarithmic scale highlights the linear growth of VecComp in L versus the exponential growth of the naïve scheme.

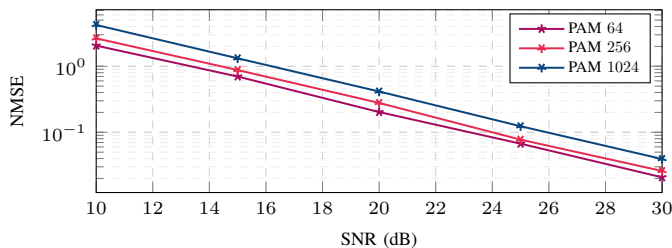


Figure 7. Performance of adapting PAM modulations over the noisy MAC. The function is the affine transform in (32) with $K = 10$ and $L = 10$, where coefficients $a_{\ell,k}$ are generated randomly from $\{0, 1, \dots, Q - 1\}$. The figure shows the performance for different SNRs and the modulation order when the SNR = 10 dB over 5×10^3 Monte Carlo trials.

with ChannelComp. In contrast, MIMO SumComp does not incur any optimization overhead, as it admits a closed-form solution for modulation mapping. The naïve extension of ChannelComp, however, exhibits exponential growth in L , with ratios that increase rapidly on the logarithmic scale. These results highlight that VecComp achieves substantial computational savings: it preserves the same order of complexity as ChannelComp in q and K , while scaling with a linear factor L .

E. Computation Performance for Affine Transform

We study the performance of the computation over the noisy MAC, for computing an affine function in (32), where $a_{k,\ell}$ are generated randomly from the set $\{0, 1, \dots, Q - 1\}$ for all $(k, \ell) \in [K] \times [L]$ with $K = 50$ nodes. Furthermore, the input data \mathbf{s} is selected uniformly at random from the integers number between 0 and $Q - 1$, i.e., $s_{k,\ell} = \{0, 1, \dots, Q - 1\}$ for all $(k, \ell) \in [K] \times [L]$. We use the PAM as described in V-A for the modulation. The results are averaged over 5×10^3 Monte Carlo trials. In Figure 7, we depict the performance of the VecComp over various numbers of nodes K in terms of NMSE for PAM of orders $Q = \{4, 8, 16, 32\}$ with $L = 5$. By increasing the order of modulation Q , the MSE increases due to reducing the distance of the constellation points.

F. Computation Performance for Convolution

For the last experiment, we evaluate the computation performance of VecComp for different SNRs and modulation

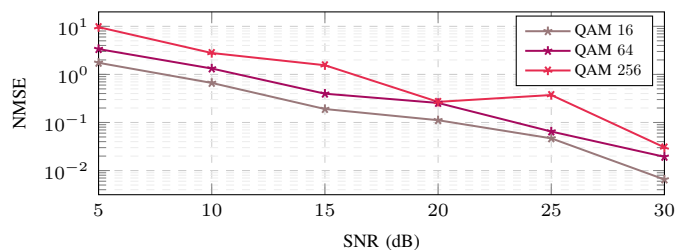


Figure 8. NMSE performance of VecComp for different QAM modulation orders $Q^2 \in \{16, 64, 256\}$ and SNR levels ranging from 5 dB to 30 dB. The results, averaged over 10^4 Monte Carlo trials, illustrate how increasing SNR improves computation accuracy across all modulation levels, while higher modulation orders (e.g., 256-QAM) show increased MSE due to their higher sensitivity to noise.

orders. For the function computation, we consider the special scenario described in Section V-B, where the desired function is the convolution, and the nodes use QAM for sending their values. This analysis examines the accuracy and robustness of the VecComp approach under various ranges of input values levels $s_{k,\ell}$ in $\{0, 1, \dots, Q\}$, where $Q \in \{4, 8, 16\}$ corresponds to QAM of order 16, 64 and 256, respectively. The SNR values tested range from 10 to 30 dB, allowing us to assess how noise and modulation complexity affect NMSE in the computation.

In each trial, we simulate the convolution operation over the noisy MAC, applying QAM modulation and demodulation to the convolution results over the noisy MAC. Also, the experiments are averaged over 10^4 Monte Carlo trials. Results are depicted in Figure 8, showing the impact of SNR on MSE across different QAM modulation orders. The higher modulation orders (e.g., 256-QAM) yield higher NMSEs due to their increased susceptibility to noise. However, as SNR increases from 10 to 30 dB, MSE decreases across all modulation levels, demonstrating that higher SNR conditions improve VecComp's accuracy and computation robustness as expected. These results confirm the trade-offs between noise resilience and modulation complexity in the digital computation framework of VecComp.

VII. CONCLUSION

This paper introduced VecComp, an extension of the ChannelComp methodology that leverages MIMO technology to enable robust vector-based computations over fading channels.

Our analysis established a non-asymptotic upper bound on the MSE of VecComp, supporting its theoretical efficacy in mitigating fading effects. Numerical experiments confirmed that VecComp effectively balances computation accuracy and resilience across various modulation orders and SNR levels. Specifically, the scaling of receiver antennas and modulation order demonstrated the adaptability of VecComp in achieving computational reliability in data-centric applications requiring vector-based computations. Furthermore, the versatility of VecComp renders it applicable to a broad range of practical scenarios. Potential applications include real-time distributed machine learning, large-scale sensor networks, IoT deployments, and task-oriented OAC, where efficient OAC is paramount.

These findings indicate that VecComp is a promising solution for enhancing computational and communication reliability in digital over-the-air vector function computations, marking a step toward scalable, reliable, and efficient distributed data processing.

APPENDIX

A. Proof of Theorem 1

Consider the target signal $\mathbf{r} := \sum_{k=1}^K \mathbf{x}_k$, we can define the error as follows:

$$\begin{aligned} \|\mathbf{r} - \mathbf{y}\|_2 &= \|\mathbf{r} - \mathbf{y}_{\text{sig}} - \mathbf{y}_{\text{inter}} - \mathbf{y}_{\text{noise}}\|_2, \\ &\leq e_{\text{sig}} + e_{\text{inter}} + e_{\text{noise}}, \end{aligned} \quad (38)$$

where

$$e_{\text{sig}} := \left\| \mathbf{r} - \frac{1}{N_r} \sum_{k=1}^K \mathbf{G}_k^H \mathbf{G}_k \mathbf{x}_k \right\|_2, \quad (39a)$$

$$e_{\text{inter}} := \left\| \frac{1}{N_r} \sum_{k,k',k \neq k'} \mathbf{G}_{k'}^H \mathbf{G}_k \mathbf{x}_k \right\|_2, \quad (39b)$$

$$e_{\text{noise}} := \left\| \frac{1}{N_r} \sum_{k=1}^K \mathbf{G}_k^H \mathbf{z} \right\|_2, \quad (39c)$$

with $\mathbf{G}_k := \mathbf{H}_k \mathbf{V}_k / N_t \in \mathbb{C}^{N_r \times L}$ is a random matrix with i.i.d. entries distributed as $\mathcal{CN}(0, 1)$. We analyze each term separately in the sequel and find how fast the tails of the error terms, e_{sig} , e_{inter} , and e_{noise} approach zero. To this end, we use the following concentration inequality for the matrix elements in error terms.

Lemma 1. (Matrix Bernstein) [54, Theorem 1.6.2], *Let $\mathbf{S}_1, \dots, \mathbf{S}_n$ be independent, centered random matrices with common dimension $d_1 \times d_2$, and assume that each matrix is uniformly bounded as*

$$\mathbb{E}[\mathbf{S}_k] = \mathbf{0}, \quad \|\mathbf{S}_k\| \leq L, \quad \text{for each } k = 1, \dots, n. \quad (40)$$

Let us introduce the sum $\mathbf{Z} = \sum_{k=1}^n \mathbf{S}_k$, and let $v(\mathbf{Z})$ denote the matrix variance statistic of the sum, defined as

$$\begin{aligned} v(\mathbf{S}) &= \max\{\|\mathbb{E}[\mathbf{Z}\mathbf{Z}^H]\|, \|\mathbb{E}[\mathbf{Z}^H\mathbf{Z}]\|\} \\ &= \max\left\{\left\|\sum_{k=1}^n \mathbb{E}[\mathbf{S}_k \mathbf{S}_k^H]\right\|, \left\|\sum_{k=1}^n \mathbb{E}[\mathbf{S}_k^H \mathbf{S}_k]\right\|\right\}. \end{aligned}$$

Then,

$$\mathbb{P}[\|\mathbf{Z}\| \geq t] \leq (d_1 + d_2) \exp\left(\frac{-t^2/2}{v(\mathbf{Z}) + Lt/3}\right) \quad \text{for all } t \geq 0$$

Corollary 1. (Expectation Upper bound) [54, Section 1.6] *Furthermore, the expectation of the spectral norm of the matrix $\mathbf{Z} \in \mathbb{R}^{d_1 \times d_2}$ can be bound as*

$$\mathbb{E}[\|\mathbf{Z}\|] \leq \sqrt{2v(\mathbf{Z}) \log(d_1 + d_2)} + \frac{1}{3}L \log(d_1 + d_2). \quad (41)$$

In the following, we use the concentration inequalities in Lemma 1 to obtain a probabilistic upper bound on each error term in (39). Consequently, we can show that the upper bound for each error term asymptotically reaches zero for a large enough number of antennas, N_r .

Lemma 2. *Let $\epsilon_1 > 0$ and $\delta_1 > 0$ be positive scalars. Then, the absolute value of the signal error $|e_{\text{sig}}|$ is upper bounded by the scalar ϵ_1 , with probability at least $1 - \delta_1$ as follows:*

$$|e_{\text{sig}}| \leq \epsilon_1, \quad \text{if } N_r \geq \frac{2\gamma L}{\epsilon_1^2} \ln\left(\frac{L+1}{\delta_1}\right), \quad (42)$$

where $\gamma = \sum_{k=1}^K \|\mathbf{x}_k\|_2^2$.

Proof. See Appendix C. \square

Lemma 3. *Let $\epsilon_2 > 0$ and $\delta_2 > 0$ be positive scalars. Then, the absolute value of the interference error, $|e_{\text{inter}}|$, is upper bounded by the scalar ϵ_2 , with probability at least $1 - \delta_2$ as follows:*

$$|e_{\text{inter}}| \leq \epsilon_2 \quad \text{if } N_r \geq \frac{2\gamma L K^2}{\epsilon_2^2} \ln\left(\frac{K(L+1)}{\delta_2}\right). \quad (43)$$

Proof. See Appendix D. \square

Lemma 4. *Let $\epsilon_3 > 0$ and $\delta_3 > 0$ be positive scalars. Then, the absolute value of the noise error, $|e_{\text{noise}}^n|$, is upper bounded by the scalar ϵ_3 with probability at least $1 - \delta_3$ as follows*

$$|e_{\text{noise}}^n| \leq \epsilon_3 \quad \text{if } N_r \geq \frac{8LK\sigma_z^2}{\epsilon_3^2} \ln\left(\frac{L+1}{\delta_3}\right). \quad (44)$$

Proof. See Appendix E. \square

The proofs of Lemmas 2, 3, and 4 are straightforward by applying Lemma 1 on the corresponding error term in (39). Hence, the proofs are omitted for brevity.

By invoking Lemmas 2, 3, and 4, we obtain an upper bound on the error terms in (38) below:

$$\|e\|_2 \leq e_{\text{sig}} + e_{\text{inter}} + e_{\text{noise}} \leq \epsilon_1 + \epsilon_2 + \epsilon_3 \leq \epsilon. \quad (45)$$

Due to the union bound, the events of Lemmas 2, 3, and 4 hold simultaneously with probability no less than $1 - (\delta_1 + \delta_2 + \delta_3)$ or $1 - \delta$, where $\delta \geq \delta_1 + \delta_2 + \delta_3$ [53]. Thus, this proves (15).

Then, all the Lemmas can be satisfied if the number of antennas at the CP is large enough, i.e.,

$$N_r \geq 2 \max \left\{ \frac{\gamma L}{\epsilon_1^2} \ln\left(\frac{L+1}{\delta_1}\right), \frac{\gamma L K^2}{\epsilon_2^2} \ln\left(\frac{K(L+1)}{\delta_2}\right), \frac{4LK\sigma_z^2}{\epsilon_3^2} \ln\left(\frac{L+1}{\delta_3}\right) \right\}. \quad (46)$$

By setting $\delta_1 = \delta/2K$, $\delta_2 = \delta/2$, and $\delta_3 = \delta/2K$, we obtain the following lower bound:

$$N_r \geq 2 \max \left\{ \frac{\gamma L}{\epsilon_1^2}, \frac{\gamma L K^2}{\epsilon_2^2}, \frac{4LK\sigma_z^2}{\epsilon_3^2} \right\} \ln\left(\frac{2K(L+1)}{\delta}\right), \quad (47)$$

where $\delta > 0$, and for any $K \geq 2$, we have

$$\delta_1 + \delta_2 + \delta_3 = \left(\frac{1}{2} + \frac{1}{2K} + \frac{1}{2K} \right) \delta \leq \delta. \quad (48)$$

For further simplifications, we reformulate ϵ_1, ϵ_2 , and ϵ_3 in terms of a positive value $\epsilon' > 0$ as follows:

$$\epsilon_1 = \frac{\epsilon'}{K\sigma_z}, \quad \epsilon_2 = \frac{1}{\sigma_z}\epsilon', \quad \epsilon_3 = \frac{2\epsilon'}{\gamma\sqrt{K}}. \quad (49)$$

Hence, it yields the following:

$$\begin{aligned} \epsilon_1 + \epsilon_2 + \epsilon_3 &\leq \epsilon' \left(\frac{1}{K\sigma_z} + \frac{1}{\sigma_z} + \frac{2}{\gamma\sqrt{K}} \right), \\ &\leq \epsilon' \left(\frac{2}{\sigma_z} + \frac{2}{\gamma} \right) \leq \frac{\epsilon'}{\min\{\sigma_z/4, \gamma/4\}} = \frac{\epsilon'}{\sqrt{c_{\sigma, \gamma}}}, \end{aligned}$$

where $c_{\sigma, \gamma} := \min\{\sigma_z^2, \gamma^2\}/16$. Substituting (49) into (47), we obtain

$$N_r \geq \frac{2c_{\sigma, \gamma} L K^2 \gamma \sigma_z^2}{\epsilon'^2} \ln \left(\frac{2K(L+1)}{\delta} \right), \quad (50)$$

with probability no less than $1 - \delta$. Hence, we conclude the proof.

B. Proof of Proposition 2

We need to prove that $\hat{\mathbf{X}}_\ell = (\hat{\mathbf{Y}}_\ell + \tilde{\mathbf{X}}_\ell)/\kappa$ satisfies all the constraints in (26). For the power constraint, we note that

$$\|\hat{\mathbf{X}}_\ell\|_{\text{F}}^2 = \frac{1}{\kappa^2} (\|\hat{\mathbf{Y}}_\ell\|_{\text{F}}^2 + \|\tilde{\mathbf{X}}_\ell\|_{\text{F}}^2) = 1. \quad (51)$$

where the first equality is due to the fact that $\langle \tilde{\mathbf{X}}_\ell, \hat{\mathbf{Y}}_\ell \rangle = 0$ for any $\tilde{\mathbf{X}}_\ell \in \mathcal{N}(\mathcal{A}_\ell^{\text{O}})$ and $\hat{\mathbf{Y}}_\ell \notin \mathcal{N}(\mathcal{A}_\ell^{\text{O}})$. Next, for the other constraint in (26), we only need to show that Algorithm 1 gives a non-orthogonal vector to the set of input vectors in the sequel. Let $\{\mathbf{v}_1, \dots, \mathbf{v}_m\}$ be a set of given vectors in \mathbb{R}^n and $\mathbf{x} = \text{NonOrth}(\mathbf{v}_1, \dots, \mathbf{v}_m)$ be the output from Algorithm 1. For $i \in \{2, \dots, K\}$, we have

$$\langle \mathbf{x}, \mathbf{v}_i \rangle = \langle \alpha \mathbf{v}_1 + \mathbf{y}, \mathbf{v}_i \rangle = \langle \mathbf{y}, \mathbf{v}_i \rangle \neq 0, \quad (52)$$

which holds due to the definition of \mathbf{y} in Algorithm 1. On the other hand, for $i \in \{k+1, \dots, m\}$, we have $\langle \mathbf{x}, \mathbf{v}_i \rangle = \alpha \langle \mathbf{v}, \mathbf{v}_i \rangle + \langle \mathbf{y}, \mathbf{v}_i \rangle \neq 0$. The last term cannot be zero because then we would have $\alpha = -\langle \mathbf{y}, \mathbf{v}_i \rangle / \langle \mathbf{v}_1, \mathbf{v}_i \rangle$. This contradicts how we selected the parameter α in Algorithm 1. Hence, $\mathbf{x} \not\perp \{\mathbf{v}_1, \dots, \mathbf{v}_m\}$.

C. Proof of Lemma 2

For each $k \in [K]$, we define the random variable $\mathbf{S}_k \in \mathbb{C}^{L \times 1}$

$$\mathbf{S}_k := \left(\mathbf{I}_L - \frac{1}{N_r} \mathbf{G}_k^{\text{H}} \mathbf{G}_k \right) \mathbf{x}_k. \quad (53)$$

Since $\mathbb{E}[\mathbf{G}_k^{\text{H}} \mathbf{G}_k] = N_r \mathbf{I}_L$, it follows immediately that $\mathbb{E}[\mathbf{S}_k] = \mathbf{0}$. Moreover, using the definition of \mathbf{r} , we have

$$\sum_{k=1}^K \mathbf{S}_k = \mathbf{r} - \frac{1}{N_r} \sum_{k=1}^K \mathbf{G}_k^{\text{H}} \mathbf{G}_k \mathbf{x}_k. \quad (54)$$

In order to invoke Lemma 1, we first derive a uniform bound on $\|\mathbf{S}_k\|_2$. By the sub-multiplicativity of the spectral norm, we

$$\begin{aligned} \|\mathbf{S}_k\|_2 &\leq \left\| \mathbf{I}_L - \frac{1}{N_r} \mathbf{G}_k^{\text{H}} \mathbf{G}_k \right\| \|\mathbf{x}_k\|_2 \\ &\leq \left(1 + \frac{1}{N_r} \|\mathbf{G}_k^{\text{H}} \mathbf{G}_k\| \right) \|\mathbf{x}_k\|_2, \\ &= \left(1 + \frac{1}{N_r} \|\mathbf{G}_k\|^2 \right) \|\mathbf{x}_k\|_2. \end{aligned} \quad (55)$$

For tall random matrices with i.i.d. circularly symmetric complex Gaussian entries, the Bai–Yin law implies that $\|\mathbf{G}_k\| \leq 2\sqrt{N_r}$ almost surely for sufficiently large N_r . Therefore,

$$\|\mathbf{S}_k\|_2 \leq \left(1 + \frac{(2\sqrt{N_r})^2}{N_r} \right) \|\mathbf{x}_k\|_2 = 5\|\mathbf{x}_k\|_2, \quad k \in [K]. \quad (56)$$

We next evaluate the variance term required by Lemma 1. From the definition of \mathbf{S}_k , we obtain

$$\mathbb{E}[\mathbf{S}_k^{\text{H}} \mathbf{S}_k] = \mathbf{x}_k^{\text{H}} \mathbb{E} \left[\mathbf{I}_L - \frac{2}{N_r} \mathbf{G}_k^{\text{H}} \mathbf{G}_k + \frac{1}{N_r^2} \mathbf{G}_k^{\text{H}} \mathbf{G}_k \mathbf{G}_k^{\text{H}} \mathbf{G}_k \right] \mathbf{x}_k.$$

Since $\mathbf{G}_k^{\text{H}} \mathbf{G}_k$ is a complex Wishart matrix, its first two moments satisfy $\mathbb{E}[\mathbf{G}_k^{\text{H}} \mathbf{G}_k] = N_r \mathbf{I}_L$ and $\mathbb{E}[\mathbf{G}_k^{\text{H}} \mathbf{G}_k \mathbf{G}_k^{\text{H}} \mathbf{G}_k] = N_r(N_r + L) \mathbf{I}_L$. Substituting these identities yields

$$\mathbb{E}[\mathbf{S}_k^{\text{H}} \mathbf{S}_k] = \mathbf{x}_k^{\text{H}} \left(\frac{L}{N_r} \mathbf{I}_L \right) \mathbf{x}_k = \frac{L}{N_r} \|\mathbf{x}_k\|_2^2. \quad (57)$$

Consequently,

$$\left\| \sum_{k=1}^K \mathbb{E}[\mathbf{S}_k^{\text{H}} \mathbf{S}_k] \right\| \leq \frac{L}{N_r} \sum_{k=1}^K \|\mathbf{x}_k\|_2^2. \quad (58)$$

Applying Lemma 1 with the bounds in (56) and (58), we obtain $\left\| \sum_{k=1}^K \mathbf{S}_k \right\|_2 \leq \epsilon_1$, with probability at least

$$1 - (L+1) \exp \left(- \frac{N_r \epsilon_1^2 / 2}{L \sum_{k=1}^K \|\mathbf{x}_k\|_2^2 + \frac{5\epsilon_1}{3} \max_k \|\mathbf{x}_k\|_2} \right). \quad (59)$$

Let $\delta_1 > 0$ be given and define $\gamma := \sum_{k=1}^K \|\mathbf{x}_k\|_2^2$. A sufficient condition for the above probability to be no smaller than $1 - \delta_1$ is

$$N_r \geq \frac{2\gamma L}{\epsilon_1^2} \ln \left(\frac{L+1}{\delta_1} \right), \quad (60)$$

which completes the proof.

D. Proof of Lemma 3

Let us define the variable $\mathbf{Z}_k \in \mathbb{C}^{L \times L}$ for $k \in [K]$ as follows:

$$\mathbf{Z}_k := \frac{1}{N_r} \sum_{k'=1, k' \neq k}^K \mathbf{G}_{k'}^{\text{H}} \mathbf{G}_k. \quad (61)$$

Next, considering the fact that the elements of \mathbf{G}_k and $\mathbf{G}_{k'}$ are statistically independent, we have $\mathbb{E}[\mathbf{Z}_k] = \mathbf{0}$, for $k \in [K]$. In order to apply Lemma 1, we need to bound the norm of each variable, $\|\mathbf{Z}_k\|_2$, and the variance term, $\|\mathbb{E}[\mathbf{Z}_k^{\text{H}} \mathbf{Z}_k]\|_2$, which we tackle separately in the following. For the norm, we have

$$\begin{aligned} \|\mathbf{Z}_k\| &\leq \frac{1}{N_r} \sum_{k'} \|\mathbf{G}_{k'}^{\text{H}}\| \|\mathbf{G}_k\| \leq \frac{K-1}{N_r} \|\mathbf{G}_k\| \|\mathbf{G}_{k'}\|, \\ &\leq \frac{K}{N_r} \|\mathbf{G}_k\|^2 \leq \frac{4N_r K}{N_r} \leq 4K, \end{aligned} \quad (62)$$

for $k \in [K]$. Since $\|\mathbf{G}_k\|$ follows Bai-Yin laws (for tall matrices $N_r \gg L$), which can be bounded by a factor $2\sqrt{N_r}$ almost surely [37]. Now, the variance term can be bounded as

$$\mathbb{E}[\mathbf{G}_k^H \mathbf{G}_{k'} \mathbf{G}_k^H \mathbf{G}_k] = N_r L \mathbf{I}_L. \quad (63)$$

Consequently, it yields

$$\left\| \mathbb{E}[\mathbf{Z}_k^H \mathbf{Z}_k] \right\| \leq \frac{(K-1)N_r L}{N_r^2} < \frac{LK}{N_r}.$$

Thus, the direct results of applying Lemma 1 to each variable \mathbf{Z}_k for $\epsilon_2 / \sum_k \|\mathbf{x}_k\| \sqrt{K}$ together with union bound give us the following upper bound:

$$\left\| \sum_{k=1}^K \mathbf{Z}_k \mathbf{x}_k \right\|_2 \leq \left(\sum_k \|\mathbf{Z}_k\|^2 \right)^{1/2} \left(\sum_k \|\mathbf{x}_k\|_2^2 \right)^{1/2} \leq \epsilon_2,$$

where the first inequality is the Cauchy-Schwarz inequality, with probability no less than

$$1 - K(L+1) \exp\left(\frac{-N_r \epsilon_2^2 \gamma^{-1}}{2LK^2 + \frac{8\epsilon_2}{\sqrt{\gamma^3}}}\right) \geq 1 - \delta_2.$$

By rearranging the expression in terms of δ_2 , we obtain

$$N_r \geq \frac{2\gamma LK^2}{\epsilon_2^2} \ln\left(\frac{K(L+1)}{\delta_2}\right), \quad (64)$$

where $\delta_2 > 0$. This concludes the proof of Lemma 3.

E. Proof of Lemma 4

Let us define the variable $\mathbf{Q}_k \in \mathbb{C}^{L \times N_r}$ for $k \in [K]$ as:

$$\mathbf{Q}_k := \frac{1}{N_r} \mathbf{G}_k^H, \quad k \in [K]. \quad (65)$$

Thus, we can check that $\mathbb{E}[\mathbf{Q}_k] = \mathbf{0}$. Following the same strategy for the proof in Appendix D, we first bound $\|\mathbf{Q}_k\|_2$ as follows:

$$\|\mathbf{Q}_k\| \leq \frac{1}{N_r} \|\mathbf{G}_k\| \leq \frac{2\sqrt{N_t}}{N_r} = \frac{2}{\sqrt{N_r}},$$

for $k \in [K]$. Then, we tackle the variance below:

$$\mathbb{E}[\mathbf{Q}_k^H \mathbf{Q}_k] = \mathbb{E}\left[\frac{1}{N_r^2} \mathbf{G}_k^H \mathbf{G}_k\right] = \frac{L \mathbf{I}_{N_r}}{N_r^2}. \quad (66)$$

Hence, we obtain

$$\left\| \sum_k \mathbb{E}[\mathbf{Q}_k^H \mathbf{Q}_k] \right\| \leq \frac{KL}{N_r^2} \leq \frac{K}{N_r}. \quad (67)$$

Similarly, Lemma 1 gives us the following error bound.

$$\left\| \sum_{k=1}^K \mathbf{Q}_k \mathbf{z} \right\|_2 \leq \left\| \sum_{k=1}^K \mathbf{Q}_k \right\| \|\mathbf{z}\|_2 \leq \epsilon_3, \quad (68)$$

for $N_r \geq \frac{8LK\sigma_z^2}{\epsilon_3^2} \ln\left(\frac{L+1}{\delta_3}\right)$, with probability at least $1 - \delta_3$. Here, we used the fact that $\|\mathbf{z}\| \leq 2\sqrt{L}\sigma_z$ almost surely. As a result, we can conclude the proof of Lemma 4.

F. Proof of Theorem 2

Under imperfect CSI, the distortion term $\Delta \mathbf{y}$ in (18) can be decomposed into an interference-type component and a noise-type component, i.e., $\Delta \mathbf{y} = e'_{\text{inter}} + e'_{\text{noise}}$. To characterize these two components, define

$$\bar{\mathbf{Z}}_k := \frac{1}{N_r} \sum_{k'=1, k' \neq k}^K \bar{\mathbf{G}}_{k'}^H \mathbf{G}_k \in \mathbb{C}^{L \times L}, \quad (69a)$$

$$\bar{\mathbf{Q}}_k := \frac{1}{N_r} \bar{\mathbf{G}}_k^H \in \mathbb{C}^{L \times N_r}, \quad k \in [K], \quad (69b)$$

results in $e'_{\text{inter}} = \sum_k \bar{\mathbf{Z}}_k$ and $e'_{\text{noise}} = \sum_k \bar{\mathbf{Q}}_k$, where $\bar{\mathbf{G}}_k := \frac{1}{N_t} \Delta \mathbf{H}_k \mathbf{V}_k \in \mathbb{C}^{N_r \times L}$ whose entries are i.i.d. and distributed as $\mathcal{CN}(0, \xi_k^2)$ with $\xi_k = \sigma_{I,k} / \sigma_{h,k}$.

Since the estimation errors $\Delta \mathbf{H}_k$ are mutually independent across nodes and are independent of the true channel matrices \mathbf{H}_k , it follows that $\mathbb{E}[\bar{\mathbf{Z}}_k] = \mathbf{0}$ and $\mathbb{E}[\bar{\mathbf{Q}}_k] = \mathbf{0}$. Hence, the matrix Bernstein inequality in Lemma 1 can be applied in the same manner as in Lemmas 3 and 4 for the random matrices $\bar{\mathbf{Z}}_k$ and $\bar{\mathbf{Q}}_k$, respectively. Following the arguments in Lemma 3, we obtain $\|\bar{\mathbf{Z}}_k\| \leq \sum_{k', k' \neq k} 4K \xi_{k'} \leq 4K \sum_{k=1}^K \xi_k$, where the last inequality holds since $\xi_k \geq 0$. Moreover, the corresponding variance term satisfies $\|\mathbb{E}[\bar{\mathbf{Z}}_k^H \bar{\mathbf{Z}}_k]\| \leq L \sum_{k=1}^K \xi_k^2 / N_r$. As a consequence, for any $\epsilon_4 > 0$ and $\delta_4 \in (0, 1)$, $\left\| \sum_{k=1}^K \bar{\mathbf{Z}}_k \mathbf{x}_k \right\|_2 \leq \epsilon_4$ holds with probability at least $1 - \delta_4$ provided that

$$N_r \geq \frac{2\gamma LK \sum_k \xi_k^2}{\epsilon_4^2} \ln\left(\frac{K(L+1)}{\delta_4}\right).$$

Next, by applying the same steps as in Lemma 4 to the matrices $\bar{\mathbf{Q}}_k$, we obtain $\|\bar{\mathbf{Q}}_k\| \leq \frac{2\xi_k}{\sqrt{N_r}}$, and $\left\| \sum_{k=1}^K \mathbb{E}[\bar{\mathbf{Q}}_k^H \bar{\mathbf{Q}}_k] \right\| \leq \frac{1}{N_r} \sum_{k=1}^K \xi_k^2$. Therefore, for any $\epsilon_5 > 0$ and $\delta_5 \in (0, 1)$, $\left\| \sum_{k=1}^K \bar{\mathbf{Q}}_k \mathbf{z} \right\|_2 \leq \epsilon_5$ with probability at least $1 - \delta_5$, provided that

$$N_r \geq \frac{8L\sigma_z^2 \sum_k \xi_k^2}{\epsilon_5^2} \ln\left(\frac{L+1}{\delta_5}\right).$$

To guarantee that both components of $\Delta \mathbf{y}$ are bounded and that $\|\Delta \mathbf{y}\|_2 \leq \epsilon''/2$ holds with probability at least $1 - \delta/2$, we combine the above two bounds using the same union bound arguments as in (45)–(50). This yields the sufficient condition

$$N_r \geq \frac{8c_{\sigma, \gamma} LK^2 \gamma \sigma_z^2 \bar{\xi}}{\epsilon''^2} \ln\left(\frac{4K(L+1)}{\delta}\right), \quad (70)$$

where $\bar{\xi} = \sum_{k=1}^K \xi_k^2 / K$. Finally, by invoking Theorem 1 and the resultant lower bound in (70), while setting $\epsilon''/2$ in (16), we obtain

$$\|\mathbf{r} - \hat{\mathbf{r}}\|_2 \leq \|\mathbf{y}\|_2 + \|\Delta \mathbf{y}\|_2 \leq \epsilon''/2 + \epsilon''/2 = \epsilon'',$$

with probability at least $1 - \delta$, provided that

$$N_r \geq \frac{8c_{\sigma, \gamma} LK^2 \gamma \sigma_z^2 \max\{\bar{\xi}/K, 1\}}{\epsilon''^2} \ln\left(\frac{4K(L+1)}{\delta}\right).$$

This completes the proof.

REFERENCES

- [1] B. Nazer and M. Gastpar, "Computation over multiple-access channels," *IEEE Trans. Info. Theo.*, vol. 53, no. 10, pp. 3498–3516, 2007.
- [2] H. Hellström *et al.*, "Wireless for machine learning: A survey," *Foundations and Trends® in Signal Processing*, vol. 15, no. 4, 2022.
- [3] M. Goldenbaum *et al.*, "Harnessing interference for analog function computation in wireless sensor networks," *IEEE Trans. Sig. Proc.*, vol. 61, no. 20, pp. 4893–4906, 2013.
- [4] M. Gastpar, "Uncoded transmission is exactly optimal for a simple Gaussian sensor network," *IEEE Trans. Info. Theo.*, vol. 54, no. 11, pp. 5247–5251, 2008.
- [5] G. Zhu *et al.*, "One-bit over-the-air aggregation for communication-efficient federated edge learning: Design and convergence analysis," *IEEE Trans. Wireless Commun.*, vol. 20, no. 3, pp. 2120–2135, 2020.
- [6] S. Razavikia *et al.*, "ChannelComp: A general method for computation by communications," *IEEE Trans. on Commun.*, vol. 72, no. 2, pp. 692–706, 2023.
- [7] —, "SumComp coding: Digital over-the-air computation via the ring of integers," *IEEE Trans. on Commun.*, 2024.
- [8] A. Adjoudani *et al.*, "Prototype experience for MIMO BLAST over third-generation wireless system," *IEEE J. Select. Areas Commun.*, vol. 21, no. 3, pp. 440–451, 2003.
- [9] M. Goldenbaum *et al.*, "Nomographic functions: Efficient computation in clustered Gaussian sensor networks," *IEEE Trans. Wireless Commun.*, vol. 14, no. 4, pp. 2093–2105, 2014.
- [10] B. Nazer and M. Gastpar, "Compute-and-forward: Harnessing interference through structured codes," *IEEE Trans. Info. Theo.*, vol. 57, no. 10, pp. 6463–6486, 2011.
- [11] M. Goldenbaum and S. Stanczak, "Robust analog function computation via wireless multiple-access channels," *IEEE Trans. on Commun.*, vol. 61, no. 9, pp. 3863–3877, 2013.
- [12] S. Razavikia *et al.*, "Blind asynchronous over-the-air federated edge learning," in *Globecom Workshops*. IEEE, 2022, pp. 1834–1839.
- [13] H. Hellström *et al.*, "Optimal receive filter design for misaligned over-the-air computation," in *Globecom Workshops*. IEEE, 2023, pp. 1529–1535.
- [14] M. M. Amiri and D. Gündüz, "Federated learning over wireless fading channels," *IEEE Trans. Wireless Commun.*, vol. 19, no. 5, pp. 3546–3557, 2020.
- [15] A. Şahin, "Over-the-air computation based on balanced number systems for federated edge learning," *IEEE Trans. on Wireless Commun.*, 2023.
- [16] G. Zhu *et al.*, "Broadband analog aggregation for low-latency federated edge learning," *IEEE Trans. Wireless Commun.*, vol. 19, no. 1, pp. 491–506, 2019.
- [17] A. Şahin, "Over-the-air majority vote computation with modulation on conjugate-reciprocal zeros," *IEEE Trans. Wireless Commun.*, 2024.
- [18] J. Bernstein *et al.*, "signSGD: Compressed optimisation for non-convex problems," in *Int. Conf. Mach. Learn.* PMLR, 2018, pp. 560–569.
- [19] G. Zhu *et al.*, "MIMO over-the-air computation: Beamforming optimization on the Grassmann manifold," in *Proc. IEEE Global Telecommun. Conf.*, 2018, pp. 1–6.
- [20] —, "Over-the-air computing for wireless data aggregation in massive IoT," *IEEE Wireless Commun.*, vol. 28, no. 4, pp. 57–65, 2021.
- [21] X. Zhai *et al.*, "Hybrid beamforming for massive MIMO over-the-air computation," *IEEE Trans. on Commun.*, vol. 69, no. 4, pp. 2737–2751, 2021.
- [22] S. Jing and C. Xiao, "Transceiver beamforming for over-the-air computation in massive MIMO systems," *IEEE Trans. Wireless Commun.*, vol. 22, no. 10, pp. 6978–6992, 2023.
- [23] C. Chen *et al.*, "Over-the-air computation in cell-free massive mimo systems," in *IEEE International Workshop on Computer Aided Modeling and Design of Communication Links and Networks (CAMAD)*, 2024, pp. 1–6.
- [24] S. Razavikia *et al.*, "Computing functions over-the-air using digital modulations," in *IEEE ICC*, 2023, pp. 5780–5786.
- [25] —, "Blind federated learning via over-the-air q-QAM," *IEEE Trans. Wireless Commun.*, pp. 1–1, 2024.
- [26] S. Razavikia and C. Fischione, "On designing modulation for over-the-air computation—part i: Noise-aware design," *arXiv preprint arXiv:2506.15950*, 2025.
- [27] —, "On designing modulation for over-the-air computation—part ii: Pyramid sampling," *arXiv preprint arXiv:2506.16208*, 2025.
- [28] A. Pérez-Neira *et al.*, "Waveforms for computing over the air: A groundbreaking approach that redefines data aggregation," *IEEE Signal Processing Magazine*, vol. 42, no. 2, pp. 57–77, 2025.
- [29] J. Liu *et al.*, "Digital over-the-air computation: Achieving high reliability via bit-slicing," *IEEE Trans. Wireless Commun.*, 2025.
- [30] X. Yan *et al.*, "A novel channel coding scheme for digital multiple access computing," in *IEEE International Conference on Communications*, 2024, pp. 3851–3857.
- [31] —, "ReMAC: Digital multiple access computing by repeated transmissions," *IEEE Trans. on Commun.*, vol. 73, no. 10, pp. 8965–8979, 2025.
- [32] Z. Shao and S.-Y. R. Li, "Distributed optimization for wireless networks with inter-session network coding," in *IEEE International Symposium on Information Theory*, 2013, pp. 2725–2729.
- [33] S. Daei *et al.*, "Timely and painless breakups: Off-the-grid blind message recovery and users' demixing," *IEEE Trans. Info. Theo.*, 2025.
- [34] R. Heckel and M. Soltanolkotabi, "Generalized line spectral estimation via convex optimization," *IEEE Trans. Info. Theo.*, vol. 64, no. 6, pp. 4001–4023, 2017.
- [35] V. A. Marchenko and L. A. Pastur, "Distribution of eigenvalues for some sets of random matrices," *Matematicheskii Sbornik*, vol. 114, no. 4, pp. 507–536, 1967.
- [36] Z.-D. Bai and Y.-Q. Yin, "Limit of the smallest eigenvalue of a large dimensional sample covariance matrix," in *Advances In Statistics*. World Scientific, 2008, pp. 108–127.
- [37] R. Vershynin, *Introduction to the non-asymptotic analysis of random matrices*. Cambridge University Press, 2012, p. 210–268.
- [38] O. N. Feldheim and S. Sodin, "A universality result for the smallest eigenvalues of certain sample covariance matrices," *Geometric And Functional Analysis*, vol. 20, no. 1, pp. 88–123, 2010.
- [39] T. L. Marzetta, "Noncooperative cellular wireless with unlimited numbers of base station antennas," *IEEE Trans. Wireless Commun.*, vol. 9, no. 11, pp. 3590–3600, 2010.
- [40] L. Lu *et al.*, "An overview of massive MIMO: Benefits and challenges," *IEEE J. Select. Areas Commun.*, vol. 8, no. 5, pp. 742–758, 2014.
- [41] A. Lucas, "Robustness of the student t based m-estimator," *Communications in Statistics-Theory and Methods*, vol. 26, no. 5, pp. 1165–1182, 1997.
- [42] K. L. Bell *et al.*, "A bayesian approach to robust adaptive beamforming," *IEEE Transactions on Signal Processing*, vol. 48, no. 2, pp. 386–398, 2000.
- [43] C. Wang *et al.*, "On the performance of the MIMO zero-forcing receiver in the presence of channel estimation error," *IEEE Trans. Wireless Commun.*, vol. 6, no. 3, pp. 805–810, 2007.
- [44] B. Nosrat-Makouei *et al.*, "MIMO interference alignment over correlated channels with imperfect CSI," *IEEE Trans. Sig. Proc.*, vol. 59, no. 6, pp. 2783–2794, 2011.
- [45] N. Sidiropoulos *et al.*, "Transmit beamforming for physical-layer multicasting," *IEEE Trans. Sig. Proc.*, vol. 54, no. 6, pp. 2239–2251, 2006.
- [46] Z.-Q. Luo *et al.*, "Semidefinite relaxation of quadratic optimization problems," *IEEE Signal Processing Mag.*, vol. 27, no. 3, pp. 20–34, 2010.
- [47] X. Yan *et al.*, "Multi-symbol digital aircomp via modulation design and power adaptation," *IEEE Communications Letters*, vol. 30, pp. 602–606, 2025.
- [48] K. Sugihara and M. Iri, "Construction of the Voronoi diagram for 'one million' generators in single-precision arithmetic," *Proceedings of the IEEE*, vol. 80, no. 9, pp. 1471–1484, 1992.
- [49] E. G. Larsson *et al.*, "Massive MIMO for next generation wireless systems," *IEEE Communications Magazine*, vol. 52, no. 2, pp. 186–195, 2014.
- [50] D. Wen *et al.*, "Task-oriented over-the-air computation for multi-device edge ai," *IEEE Trans. Wireless Commun.*, vol. 23, no. 3, pp. 2039–2053, 2023.
- [51] M. M. Amiri and D. Gündüz, "Machine learning at the wireless edge: Distributed stochastic gradient descent over-the-air," *IEEE Trans. Sig. Proc.*, vol. 68, pp. 2155–2169, 2020.
- [52] S. G. Sanchez *et al.*, "AirNN: Over-the-air computation for neural networks via reconfigurable intelligent surfaces," *IEEE/ACM Transactions on Networking*, vol. 31, no. 6, pp. 2470–2482, 2022.
- [53] S. Razavikia *et al.*, "Reconstruction of binary shapes from blurred images via Hankel-structured low-rank matrix recovery," *IEEE Trans. on Image Processing*, vol. 29, pp. 2452–2462, 2020.
- [54] J. A. Tropp *et al.*, "An introduction to matrix concentration inequalities," *Foundations and Trends® in Machine Learning*, vol. 8, no. 1-2, pp. 1–230, 2015.